Development and application of a portable Raman device for in situ non-destructive detection of pork spoilage

Jingjing Li

Department of Food Science and Agricultural Chemistry

Faculty of Agricultural and Environmental Sciences

McGill University, Montreal

February, 2024

A thesis submitted to McGill University in partial fulfilment of the requirements of the degree of Master of Science

ABSTRACT

Pork spoilage has been a global concern because it can bring about economic loss as well as cause health hazard to consumers. While traditional methods for assessing spoilage offer accuracy, they suffer from drawbacks including long processing time, sample destruction, and laborious protocols. To develop a more rapid, non-invasive and easy-to-use approach for pork spoilage identification, we integrated a portable Raman spectrometer with machine learning algorithms for fresh and spoiled pork samples differentiation. In this thesis project, pork tenderloin and pork *musculus semimembranosus* were selected as samples to evaluate the capability of Raman spectrometer for pork spoilage detection. During 14-day preservation of pork samples at 4°C, we collected Raman spectra (785 nm) and assessed microbiological profiles at the same time. The spectral data was divided based on microbial testing into two categories: fresh and spoiled. Then chemometrics including PCA and several supervised machine learning algorithms were constructed to solve 2-group classification problem. The models collectively attained a 70% accuracy rate, with our self-developed convolutional neural networks (CNNs) deep learning algorithm surpassing this with an accuracy of over 90%. Additionally, we examined bacterial community dynamics via 16S rRNA high-throughput sequencing, unveiling a direct correlation between Raman spectral changes and bacterial composition at both the phylum and genus levels. In conclusion, this study validates the use of a portable Raman device as an effective tool for identifying pork spoilage, with implications for broader applications in the rapid detection of meat spoilage within the food industry.

RÉSUMÉ

La détérioration de la viande de porc est une préoccupation mondiale car elle peut entraîner des pertes économiques ainsi que des risques pour la santé des consommateurs. Alors que les méthodes traditionnelles d'évaluation de la détérioration offrent une précision, elles présentent des inconvénients, notamment des temps de traitement longs, la destruction des échantillons et des protocoles laborieux. Pour développer une approche plus rapide, non-invasive et facile à utiliser pour l'identification de la détérioration du porc, nous avons intégré un spectromètre Raman portable avec des algorithmes d'apprentissage automatique pour la différenciation des échantillons de porc frais et avariés. Dans ce projet de thèse, le filet de porc et le musculus semimembranosus du porc ont été sélectionnés comme échantillons pour évaluer la capacité du spectromètre Raman à détecter la détérioration du porc. Pendant la conservation des échantillons de porc pendant 14 jours à 4°C, nous avons collecté des spectres Raman (785 nm) et évalué les profils microbiologiques en même temps. Les données spectrales ont été divisées en deux catégories en fonction des tests microbiologiques : frais et avariés. Ensuite, des méthodes de chimiométrie incluant PCA et plusieurs algorithmes d'apprentissage automatique supervisés ont été construits pour résoudre le problème de classification en 2 groupes. Les modèles ont collectivement atteint un taux de précision de 70 %, avec notre algorithme d'apprentissage profond de réseaux neuronaux convolutionnels (CNNs) auto-développé dépassant cela avec une précision de plus de 90 %. De plus, nous avons examiné la dynamique de la communauté bactérienne via le séquençage à haut débit de 16S rRNA, révélant une corrélation directe entre les changements spectraux Raman et la composition bactérienne aux niveaux du phylum et du genre.

En conclusion, cette étude valide l'utilisation d'un appareil Raman portable comme outil efficace pour identifier la détérioration du porc, avec des implications pour des applications plus larges dans la détection rapide de la détérioration de la viande dans l'industrie alimentaire.

ACKNOWLEDGEMENT

I would like to sincerely appreciate my supervisor Dr. Xiaonan Lu for offering me this opportunity to join his lab and providing professional guidance and support during my master's study. Many thanks for the knowledge and skills you taught and the trust you put on me, which encouraged me to learn independence and critical-thinking. This would be meaningful for my entire life. I am highly grateful for Dr. Ashraf Ismail and Dr. Jennifer Ronholm for serving as my supervisory committee members and kindly providing help and advice on my thesis project.

I would also like to express my gratitude to Dr. Lixue Liu and Kaidi Wang who trained me and offered lots of help for this project. I am grateful for your time and advice. Thanks also go to Jinxin Liu for his great support on data analysis.

I would like to acknowledge the financial support from funding agency Natural Sciences and Engineering Research Council of Canada (NSERC).

Special appreciations for all the members in Lu Lab. Not only did you inspire me on academy, you were also kind, warm and amazing friends that made me enjoy the days here. Also, thanks for all my friends who trusted, encouraged and cheered me up all the time that helped me go through the challenging time.

Lastly, I would like to thank my beloved parents for their understanding, unconditional love and support. This journey of graduate study would not be accomplished without you.

PREFACE

This thesis was prepared by following the McGill University Thesis Preparation guidelines for graduate and postdoctoral studies. This thesis is expressed in traditional monograph-writing style, consists of five chapters: Introduction, Literature Review, Materials and Methods, Results and Discussion, and Conclusion. This work is original and has not been published previously.

CONTRIBUTION OF AUTHORS

Jingjing Li is the first author who is responsible for the entire thesis. Dr. Xiaonan Lu proposed this thesis project, and Dr. Lixue Liu and Kaidi Wang had direct advisory on the experimental plans. Establishment of deep learning models were constructed by Jinxin Liu. Jingjing Li carried out all the experiments, including sample preparation, microbiological testing, Raman spectra collection and data analysis. This thesis was edited and guided by Dr. Lu.

TABLE OF CONTENTS

LIST OF FIGURES

LIST OF TABLES

LIST OF ABBREVIATIONS

ANN	Artificial neural network
CNNs	Convolutional neural networks
CV	Computer Vision
DT	Decision tree
FAO	Food and Agriculture Organization
FTIR	Fourier transformed infrared
GC	Gas chromatography
HCA	Hierarchical cluster analysis
HPLC	High-performance liquid chromatography
IR	Infrared
LD	*Longissimus dorsi*
LDA	Linear discrimination analysis
LR	Logistic regression
MAP	Modified atmosphere packaging
MDA	Malonaldehyde
NGS	Next-generation sequencing
NIR	Near-infrared
OTU	Operational taxonomic unit
PBS	Phosphate-buffer saline
PCA	Principal component analysis
PCoA	Principal Co-ordinate Analysis
PCs	Principal components
PLS-DA	Partial least square discrimination analysis
SM	*Musculus semimembranosus*
SVM	Support vector machine
TBA	Thiobarbituric acid
TBARS	Thiobarbituric acid reactive substances
TL	Tenderloin
Trp	Tryptophan
TSA	Tryptic soy agar

Tyr	Tyrosine
TVB-N	Total volatile basic nitrogen
TVC	Total viable counts
WHC	Water-holding capacity

CHAPTER 1. INTRODUCTION

1.1 General Introduction

Pork and pork-based products have constituted a significant component of human diets for millennia. In recent decades, meat consumption has surged globally, with pork being the most consumed meat type internationally (Tao and Peng 2015). Therefore, ensuring the safety and quality of pork is of paramount importance. Owing to its richness in various nutrients, pork is highly perishable and vulnerable to microbial contamination. Such contamination precipitates a reduction in both quality and safety, engendering public health concerns (Huang et al. 2013). The meat industry is thus obligated to monitor and assess bacterial spoilage within meat products to comply with consumption sanitary standards. Although numerous traditional methods have been developed for the detection of meat spoilage, they are usually costly, time-intensive, complex, and destructive to the samples (Liu et al. 2019). In recent years, the development of rapid, portable, non-invasive and cheap analytical technique arises attention in meat spoilage detection (Kucha and Ngadi 2020).

Raman spectroscopy has demonstrated considerable promise as a technique for identifying food spoilage, possessing the advantages mentioned previously and showcasing its potential in several studies (Sowoidnich et al. 2010; Zając et al. 2017; Yang et al. 2020; Orlando et al. 2021). Esteemed for its non-destructive capabilities in biological analysis, Raman spectroscopy provides detailed insights into the structural changes occurring within samples. The technique operates on the principle of Raman scattering, which elucidates the vibrational modes of the chemical bonds or functional groups within molecules (Windom and Hahn 2013). Consequently, Raman spectroscopy is theoretically capable of detecting subtle changes in pork meat during storage,

thereby assessing its freshness. Furthermore, recent advances in multivariate statistical analyses have enhanced the efficiency of interpreting complex Raman spectra, potentially revolutionizing its applicability in the evaluation of meat spoilage.

Moreover, 16S rRNA high-throughput sequencing has emerged as a formidable method for elucidating the phylogeny and taxonomy of bacteria and archaea within varied microbial populations (Janda and Abbott 2007). It can provide reliable comprehension of bacterial communities and analyze the relationship between changes in microorganisms and pork spoilage. The understanding of microbial compositions during pork spoilage process can reveal possible microbial changes and offer insights to the metabolic process involved in pork spoilage. This thesis aims to ascertain the efficacy of Raman spectroscopy in the detection of pork spoilage and to investigate the association between Raman spectral data and bacterial compositions. Furthermore, this research endeavors to develop a Raman spectral database, which could serve as a valuable resource for future applications in the food indus

1.2 Research Hypotheses and Objective

This thesis articulates three primary hypotheses: (1) Portable Raman spectroscopy can be utilized effectively for the acquisition of time-series Raman spectral data. (2) Such spectra can be categorized and differentiated on the basis of microbial load and the extent of spoilage. (3) Raman spectral data are amenable to analysis through machine learning algorithms, enabling the formulation of predictive models for the precise evaluation of meat spoilage.

To validate the proposed hypotheses, the research delineates three corresponding objectives: (1) To systematically gather microbe-related test data and Raman spectra throughout the storage timeline. (2) To conduct a thorough analysis of the Raman spectra in conjunction with sequencing data. (3) To construct a comprehensive database and to engineer an advanced deep learning algorithm for the expeditious identification of pork spoilage.

CHAPTER 2. LITERATURE REVIEW

2.1 Introduction of pork spoilage

2.1.1 Importance of pork spoilage detection

Pork and its products are one of the most consumed meat products around the world owing to its property of containing relatively high levels of minerals, polyunsaturated fatty acids, essential amino acids and vitamins that are of vital importance to maintain human health (Hu et al. 2022). According to the statistics from Food and Agriculture Organization of the United Nations (FAO), global pig meat production output was 124.6 million tonnes in 2022, increasing by 1.8 percent from 2021 and accounting for about 46 percent of global meat production output. Such escalating demand for pork has catalyzed considerable advancements in the meat industry and intensified consumer emphasis on meat safety and quality (Zhao et al. 2022a).

The rich nutrients in pork meat provide a potential breeding ground for undesirable bacteria, making it vulnerable to microorganisms spoilage and lipid oxidation and resulting in off-flavors, discoloration, gas and slime production (Zhang and Peng 2016; Godziszewska et al. 2017). In the United States alone, the economic toll of pork spoilage on the meat industry is estimated to surpass 1 billion US dollars annually (Li et al. 2022a). Moreover, the degradation of pork due to biochemical reactions and microbial metabolic activity poses not only a financial burden but also a significant health risk to consumers (Huang et al. 2014). Therefore, it is necessary to evaluate the freshness of pork to assure its quality and safety throughout all stages of meat production, transportation and storage phases (Li et al. 2016a).

2.1.2 Influencing factors of pork spoilage

While meat quality losses could be implicated by multiple agents, such as microbiological metabolism, actions of enzymes, chemical reactions and physical changes, spoilage caused by

bacteria metabolic activities is the major concern (Pellissery et al. 2020; Gu et al. 2021). Microbiological contamination originates from animal microbiota, processing environment and human manipulations, and the spoilage status is related to the types and amount of microorganisms under particular storage conditions (Gill 1983; Nychas et al. 2008). Previous studies have demonstrated that bacteria are the predominant spoilage microorganisms in meat. Although yeasts and molds are also present, they are rarely monitored because they are described as subdominant microbiota, and can be detected mainly after long storage period (Chaillou et al. 2015). Among all the factors that would influence the diversity and abundance of microbiome during meat spoilage, temperature and packaging are considered as the paramount ones (Doulgeraki et al. 2012).

2.1.2.1 Storage temperature

Temperature below the optimum temperature range of microbial growth can retard microbiological propagation and achieve the prevention of spoilage. Traditional preservation methods, such as chilled and frozen storage, have been in practice for decades (Lu et al. 2019). Chilled storage (-1.5 to 5°C) typically extends the meat's freshness for a few weeks. Despite the reduced temperature, oxidative and microbial degradation continues to a certain extent, rendering it suitable for short-term preservation only. (Coombs et al. 2017; Yuan et al. 2023). Conversely, frozen storage at -18°C is a long-standing solution for extended preservation, spanning several months to over a year (Muela et al. 2010; Soyer et al. 2010; Pinheiro et al. 2019). This method, however, is not without drawbacks, as ice crystal formation can cause cellular damage and muscle deterioration, adversely affecting water holding capacity and color stability (Soyer et al. 2010; Leygonie et al. 2012). In addition to these established methods, superchilling, which entails reducing the temperature of food products to 1-2°C below their initial freezing point, has garnered significant attention in recent years (Duun and Rustad 2007). This technology combines the

beneficial effects of low temperature with conversion of only partial water into ice, which makes it less susceptible to the deteriorative process (Kaale et al. 2011). Although there are many choices for storage temperature, refrigerated (4°C) pork is the most commonly form of raw pork sale in the market because it owns superior quality in tenderness, juiciness, flavor and color (Wang et al. 2021c). Moreover, this storage condition is effective in deactivating enzymes and slowing biochemical decay, consequently extending the shelf-life of the product.

2.1.3 Packaging condition

Packaging exerts a significant influence on meat quality, with the primary packaging techniques categorized into air-permeable, vacuum, and modified atmosphere packaging (MAP) (McMillin 2008). Air-permeable packaging employs films designed with perforations that facilitate oxygen diffusion from the atmosphere, thereby creating an aerobic environment that can hasten spoilage through the proliferation of *Pseudomonas* species (Doulgeraki et al. 2012; McMillin 2017). Vacuum packaging is an effective technique for raw meat preservation based on the removal of surrounding atmosphere from the pack to maintain vacuum. The wrapping material in vacuum packaging is impermeable and serves as a barrier between outside the environment and within the container. Nonetheless, this condition would promote the dominance of obligate and facultative anaerobes including lactic acid bacteria and *B. thermosphacta* (Enfors et al. 1979). As opposed to vacuum packaging, MAP replace the original gaseous environment by flushing three principal gases: nitrogen (to avoid the oxidation of lipids), carbon dioxide (to inhibit microbial growth) and oxygen (to prevent the reproduction of anaerobes) (Narasimha Rao and Sachindra 2002). These gases are used in combination with varying proportions to impart the desirable meat quality.

2.1.4 Indicators of pork spoilage

2.1.4.1 Physical and chemical indexes

As spoilage progresses, microbial activity and endogenous enzymatic actions precipitate alterations in both the physical properties and chemical composition of meat. These transformations are manifest in several physicochemical parameters including pH, water-holding capacity (WHC), color (L*, a*, b*), levels of thiobarbituric acid reactive substances (TBARS), and total volatile basic nitrogen (TVB-N) content (Díaz et al. 2008; Coombs et al. 2017; Bekhit et al. 2021).

The pH value is a widely recognized and reliable gauge of meat freshness, with the pH of fresh meat generally ranging between 5.8 and 6.2 (Waimin et al. 2022). A pH exceeding 6.5 is indicative of spoilage and represents a potential health hazard. Throughout the maturation of meat products, including pork, there is a hydrolytic breakdown of muscle proteins into ammonia, amines, and other alkaline compounds, culminating in an elevated pH (Liu et al. 2019).

Water-holding capacity describes the ability of muscle to retain moisture, which is also a key quality parameter and has profound impacts on the tenderness, firmness and juiciness of meat products (Bowker and Zhuang 2015). The underlying mechanisms of WHC are intricately linked to muscle proteins, especially myofibrillar proteins, which bind and immobilize water within the muscle structure (Huff-Lonergan and Lonergan 2005). Throughout the postmortem aging process, proteolysis and denaturation of proteins impact on water forced out of the muscle fibers and expelled into the surroundings (Koomkrong et al. 2017; Zhang et al. 2023). Traditionally, WHC is either measured as drip loss or ultimately observed as purge in fresh meat packaging (Kapper et al. 2014). Elevated drip loss negatively impacts the visual appeal and textural quality of pork, resulting in decreased consumer acceptance and potential rejection.

Color perception notably affects consumer purchasing decisions regarding pork, with brightness often equated with freshness and quality (Norman et al. 2004). Colorimetric analysis, typically articulated in CIE parameters such as lightness (L*), redness (a*), yellowness (b*), and

color difference (E*), facilitates objective assessments. There is an established positive correlation between the a* value, indicating redness, and consumer favorability; a bright red hue is generally favored (Holman et al. 2016). As the storage time prolongs, meat discoloration occurs, correlated with the redox states of myoglobin derivatives—namely deoxyhemoglobin, oxymyoglobin, and metmyoglobin (Zhang and Peng 2016). Furthermore, these shifts in myoglobin are closely associated with oxidative changes and the proliferation of spoilage-specific microorganisms (Motoyama et al. 2010).

Thiobarbituric acid reactive substances (TBARS) are indicative of the extent of lipid oxidation, a process of critical concern as it drives the development of rancid odors and surface browning in meat (Wu et al. 2016). TBARS test is to determine the extent of formation of malonaldehyde (MDA), which is the most important and abundant aldehyde among the degradation products of lipid peroxides derived from the oxidation of polyunsaturated fatty acids (Wenjiao et al. 2014). This assay operates on the principle that MDA reacts stoichiometrically with thiobarbituric acid (TBA) to form a pink MDA-TBA adduct, the intensity of which can be measured spectrophotometrically. Consequently, the TBARS value serves as a quantitative metric for assessing the freshness of pork based on the degree of lipid oxidation (Kucha and Ngadi 2020).

Total volatile basic nitrogen (TVB-N) refers to the volatile substances that contain alkaline nitrogen, including ammonia (NH_3), dimethylamine nitrogen [$(CH_3)_2NH$], and trimethylamine nitrogen [$(CH_3)_3N$] (Prabhakar et al. 2019). These compounds arise from the breakdown of proteins and nitrogenous substances, resulting in the formation of organic amines (Bekhit et al. 2021). Specifically, as proteins in pork degrade, they yield low molecular weight metabolites such as histamine, tyramine, putrescine, and tryptamine (Yang et al. 2017). These metabolic byproducts are implicated in off-flavors and sensory displeasure, with their increasing

concentration correlating with the progression of meat spoilage. Thus, TVB-N serves as a critical indicator for evaluating the extent of meat spoilage (Leng et al. 2021).

2.1.4.2 Microbial profiles

Total viable counts (TVC) of bacteria serve as a critical microbiological metric for assessing the hygienic quality and safety of meat, as well as for monitoring spoilage over time. The acceptable limits for TVC vary by country and region. In the European Union, TVC of mechanically separated meat should be less than 5×10^6 CFU/g (EC No. 2073/2005). In China, according to GB/T 9959.2-2008, the limit of TVC in meat is $< 1 \times 10^6$ CFU/g. Similarly, in Australia, the TVC standard for hygienic meat and meat products is recommended as $< 1 \times 10^6$ CFU/g or CFU/cm^2 (AS 4696:2007) (Kim and Jang 2018). As a consequence, it has been commonly established that the critical value of TVC in relation to the spoilage is 10^6 CFU/g (Wang et al. 2012). Surpassing this benchmark can lead to discernible deterioration in meat quality and pose risks to consumer health (Barbin et al. 2013; Tao and Peng 2015).

As TVC increase during the storage period, the microbial communities also undergo shifts and succession, reflecting on the changes of predominant microorganisms. Several studies were conducted using 16S rRNA sequencing to reveal the bacterial community profiles of pork samples during preservation at 4°C (Li et al. 2019; Zhou et al. 2020; Wang et al. 2021c; Zhao et al. 2022b). While specific predominant genera identified vary across studies, a consensus is observed at the phylum level, with Proteobacteria and Firmicutes consistently representing the highest relative abundances. At the genus level, *Pseudomonas* spp., *Acinetobacter* spp., *Photobacterium* spp., and *Brochothrix* spp. are recurrently recognized. Variability in these studies likely arises from a multitude of factors, including environmental conditions, storage duration, atmospheric exposure, meat source and cut, as well as the inherent heterogeneity of meat samples. Profiling microbial communities is instrumental in identifying sources of contamination and targeting specific

bacterial growth, thus informing the development of preservation techniques designed to manage the predominant spoilage microorganisms effectively.

2.2 Detection technologies of pork spoilage

The assessment of pork quality can be characterized as the evaluation of various attributes that determine its safety for consumption over a certain period (Taheri-Garavand et al. 2019). Physical, chemical, and microbiological indicators, indicative of freshness, have been explored in the preceding section. Utilizing these indicators, a range of robust methods have been established for assessing pork freshness and identifying spoilage.

Conventional methods for determining meat quality are generally divided into subjective and objective approaches (Wu et al. 2022). Subjective methods rely heavily on human sensory assessment, drawing on an inspector's experience to evaluate aspects like color, smell, flavor, and tenderness. Despite offering immediate feedback, such evaluations are inherently laborious and biased, with outcomes often influenced by the inspector's level of fatigue (Limbo et al. 2009). In contrast, objective methods involve laboratory-based microbial assays and physicochemical analyses using specialized equipment. Microbial assessments typically include culturing in controlled conditions and colony counting, while devices such as pH meters and colorimeters gauge physical and chemical attributes (Elmasry et al. 2012). These techniques offer improvements over sensory methods in terms of accuracy and repeatability (Kamruzzaman et al. 2015). However, they are not without their challenges, including potential sample destruction, the necessity for trained personnel, and significant time investment (Khaled et al. 2021). To accommodate the modern meat industry's need for automation and high-throughput processing, novel rapid and non-destructive techniques have been developed for efficient quality assessment.

In recent years, heightened consumer consciousness regarding food safety and advancements in computer science have paved the way for the integration of artificial

intelligence in non-invasive quality assessment methods (Cheng et al. 2017). Consequently, various non-destructive technologies have been employed as effective instruments for evaluating pork spoilage, including sensor technology, computer vision, and spectroscopy (Shi et al. 2021).

Sensor techniques incorporate a suite of sensors designed for detecting odors, tastes, or patterns, notably through the application of electronic noses (E-nose) and electronic tongues (E-tongue) (Munekata et al. 2023). These devices are engineered to replicate human sensory functions, effectively identifying volatile compounds and profiling taste-related signals. Researchers have thus leveraged E-nose and E-tongue systems to quantify total viable counts (TVC) and total volatile basic nitrogen (TVB-N) in pork, providing a metric for freshness (Gil et al. 2011; Wang et al. 2012; Li et al. 2016b; Chen et al. 2019). Despite these applications, the analytical scope of E-nose and E-tongue technologies remains limited, often providing a narrow range of detection indices that may not fulfill the requirements for a comprehensive, multi-index evaluation (Shi et al. 2021).

Computer vision (CV) technology captures spatial data through digital imagery, supplanting the need for human visual assessment, and is adept at extracting features such as color, size, marbling, and other textural attributes of the meat's surface (Girolami et al. 2013). A typical CV setup includes a camera, controlled lighting, a computer, and specialized image processing software. This technology has been successfully deployed for evaluating pork color and marbling, assessing pork freshness, and estimating the quality of both pork and poultry meats (Xiao et al. 2014). Nonetheless, CV technology has a notable limitation; it is constrained to external and surface characteristics and does not yield insights into the internal composition of the sample (Taheri-Garavand et al. 2019).

Spectroscopic techniques are among the most advanced for detecting spoilage in food and meats, as alterations in meat constituents produce distinct spectral fingerprints. These methods are frequently coupled with chemometric approaches and multivariate statistical analyses to yield an extensive data analysis. Within the scope of meat spoilage detection, several spectroscopic technologies have been employed, including near-infrared (NIR) spectroscopy (Horváth et al. 2008; Balage et al. 2015; Kucha and Ngadi 2020), Fourier transform infrared (FTIR) spectroscopy (Papadopoulou et al. 2011; Zając et al. 2017; Fengou et al. 2019), Raman spectroscopy (Sowoidnich et al. 2010; Yang et al. 2020), and hyperspectral imaging (HSI) (Barbin et al. 2013; Dissing et al. 2013; Huang et al. 2013; Feifei et al. 2015; Zheng et al. 2017). Each technique offers unique benefits and their applicability within the meat industry has been validated.

Raman spectroscopy, in particular, enjoys the advantage of minimal interference from water molecules, which exhibit weak Raman scattering, thus avoiding the strong interference signals commonly encountered in NIR or FTIR (Santos et al. 2018). Furthermore, the database for Raman peak assignment is well-established, facilitating the identification of chemical structures within biological tissues. The convergence of advancements in stoichiometry and computational technology has enabled the widespread application of Raman spectroscopy in meat spoilage detection (Talari et al. 2015). However, to optimize its potential, more rigorous research is required to establish repeatable and robust analytical models. Taken together, Raman spectroscopy shows distinguished potential as a rapid and promising technique for pork spoilage or freshness identification, also to explore microbial and quality change during preservation. More details of Raman spectroscopy will be introduced in the following section.

2.3 Raman spectroscopy

Raman spectroscopy was first introduced in the first half of 20th century by the Nobel laureate Chandrasekhara Venkata Raman and Grigorij Samuilovič Landsberg (Orlando et al. 2021), but it was established after the development of laser light equipment implementation in the second half of the century. As a non-destructive analytical technique, Raman spectroscopy is highly versatile, suitable for both laboratory and field conditions, and adept at detecting structural changes in diverse sample states, including solids and liquids. Renowned for its rapid, straightforward, and non-invasive approach, the application of Raman spectroscopy has expanded significantly, finding utility in the analysis of agricultural products (Yang and Ying 2011), and branching out to various other industries, including food safety and the textile sector (V et al. 2019).

2.3.1 Mechanism and instrumentation

The fundamental mechanism of Raman spectroscopy is based upon the inelastic scattering of photons, also referred to as Raman scattering. Unlike elastic scattering, in which the frequency of the scattered light is the same as incident photon, Raman scattering results in the emission of photons with shifted frequency due to the interactions between incident light and vibrational energy of the molecules (Windom and Hahn 2013). The energy gap between incident and Raman-scattered photon is termed as Raman shift or wavenumber, which describes the vibrational modes of chemical bond or functional group within the molecule. Raman scattering occurs when a molecule vibrational mode is excited by incident light and cause deformation in electron cloud, thereby result in a change in polarizability. Raman spectrum is a plot of the intensity of the scattered light as a function of Raman shift. Usually, Raman spectra are plotted in units of intensity (which can be arbitrary) versus Raman shift in wavenumbers (cm^{-1}) so that data can be easily compared even different frequencies of the incident light are used. Since Raman shift is unique

within each molecule, Raman spectra can depict the molecular composition and structure of a targeted material thus to provide fingerprinting information of the sample.

Raman spectrum is divided into two regions: the fingerprint region that ranges from 400 to 1800 cm^{-1} and high wavenumber region ranging from 2800 to 3800 cm^{-1} (E. Masson et al. 2018). The majority of Raman spectroscopic studies for biomedical applications focus on the fingerprinting region, which is rich in biochemical information associated with proteins, lipids, nucleic acids and carbohydrates (Haka et al. 2009; O'Brien et al. 2017). To be more specific, characteristic bands associated with proteins are amide I to VII (I: 1600–1690 cm^{-1}, II: 1480–1580 cm^{-1}, III: 1230–1300 cm^{-1}, IV: 625–770 cm^{-1}, V: 640–800 cm^{-1}, VI: 540–600 cm^{-1}, VII: 200 cm^{-1}) (Rygula et al. 2013). Wavenumber region between 1050 and 1500 cm^{-1} is related to lipids and the most typical features of Raman spectra of lipids are involved with the presence of hydrocarbon chain (Czamara et al. 2015). Spectral bands at 800-1200 cm^{-1} are assigned to stretching vibrations of the OH, CH/CH_2 and C-O/C-C groups in carbohydrates (Wiercigroch et al. 2017). Except for the fingerprinting region, high wavenumber regions also contain valuable information corresponding to the vibration of the analytes, which is complementary to the patterns found in the fingerprinting region. The assignment of most common Raman bands in biological tissues have been summarized by numerous studies, which can serve as a library for the interpretation and analysis of Raman peaks (Talari et al. 2015).

In comparison with its counterpart Rayleigh scattering, Raman scattering could rarely occur with low probability. Its increasing application is mainly attributed to the development of highly efficient laser source, sensitive detectors, valid Rayleigh filter and high-throughput optics (Chase 1994). The instrumentation of modern Raman spectroscopy is usually composed of light source, filter, monochromator, sample holder and detector. A schematic diagram of Raman spectrometer is shown in **Figure 2.1**. Several types of excitation lasers have been used in Raman spectrometer,

such as argon ion (488.0 and 514.5 nm), krypton ion (530.9 and 647.1 nm), He:Ne (632.8 nm), Nd:YAG (1064 nm and 532 nm) and diode laser (Das and Agrawal 2011). Among these, diode laser source is more commonly applied to biological tissues because they can provide a higher energy efficiency than gas-based laser (Angel et al. 1995; Müller et al. 2013). In biological studies, particularly live cells, NIR lasers especially at 785 nm and 830 nm are most extensively utilized as the excitation light. This is due to the fact that NIR laser can reduce the chance of fluorescence interference, as well as they have a lower photon energy that does not cause substantial photodamage to the samples (Butler et al. 2016; Wang et al. 2018b).

Besides, there are two major technologies used to collect Raman spectra: namely dispersive Raman spectroscopy and Fourier transform Raman spectroscopy. They are different in laser source and how they detect and analyze Raman scattering signals. Both techniques have unique advantages and application scenarios (Das and Agrawal 2011). When selecting Raman spectroscopic instrumentation, factors such as sample characteristics, output requirement and others should be all taken into consideration to achieve an ideal result.

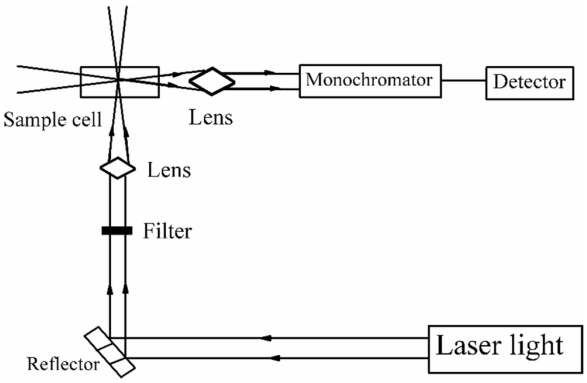

Figure 2.1 A schematic diagram of Raman spectroscopic system (Wang et al. 2018b).

2.3.2 Advantages of Raman spectroscopy in food applications

Traditional analytical methods like high-performance liquid chromatography (HPLC), gas chromatography (GC), and their mass spectrometry-coupled variants, along with atomic

absorption spectrometry, have seen widespread use in detecting and identifying components in agricultural and food products (Yang and Ying 2011). Although these methods are powerful and accurate, they are time-consuming, slow, invasive, and require strict sample pretreatment process or professional operation (Jin et al. 2016). Spectral analysis techniques such as infrared spectroscopy (IR), fluorescence spectroscopy, and Raman spectroscopy, offer a contrast by being rapid, non- or less-destructive, and more cost-effective. IR is intensively interfered by water in biological samples because water has strong absorption bands in IR, and fluorescence spectroscopy is only limited to the samples that have fluorescence effects. In contrast, water, the main constituent in food samples, only generates weak Raman signals and therefore exhibits much less interference with Raman spectra (Li and Church 2014). This feature provides Raman spectroscopy significant advantages over IR spectroscopy in aqueous and biochemical studies. Besides, Raman spectroscopy is also well known for its minimum sample preparation procedure and easy-to-use operation process. Additionally, Raman spectra can cover a wide range of 100-4000 cm^{-1}, which reveal abundant compositional and structural knowledge. The concentration-dependent nature of Raman peaks further enables quantitative analysis (Wang et al. 2021a). These benefits, coupled with the advancement of intelligent data processing algorithms, have propelled Raman spectroscopy to the forefront of applications in agricultural and food science (Sun et al. 2022).

2.3.3 Application of Raman spectroscopy in food spoilage detection

Rapid detection of food spoilage is crucial, and Raman spectroscopy has emerged as a potent technique for quality assessment and spoilage characterization through microbial load analysis. A wealth of research has affirmed Raman spectroscopy's efficacy in identifying spoilage across various food categories, including meats (Sowoidnich et al. 2010; Argyri et al. 2013; Cheng and Sun 2015; Zając et al. 2017; Jaafreh et al. 2018, 2019; Yang et al. 2020; Kim et al. 2021; Liu et

al. 2023), fruit (Guo et al. 2021b; Cai et al. 2023), beverage (Rodriguez et al. 2013; Uusitalo et al. 2017), and vegetables (Sachdev et al. 2016). Among these applications, the application in meat is more investigated since Raman spectra are sensitive to the changes in proteins and lipids that can be considered as the markers of meat spoilage. To further understand and evaluate its performance, several representative studies related to identification of meat spoilage using Raman spectroscopy will be introduced below.

Sowoidnich and co-workers used a portable 671-nm Raman spectroscopic device for rapid meat spoilage detection of porcine *musculus longissimus dorsi* (LD) and *musculus semimembranosus* (SM) (Sowoidnich et al. 2012). In this study, meat samples were stored at 5°C for 3 weeks. A series of time-dependent Raman spectra were collected, and the spectral data were analyzed by principal component analysis (PCA). The separation in PCA plot for both LD and SM coincided with the time slot around the 7 post-mortem day when bacterial surface load exceeded 10^6 CFU/cm^2. Thus, the researchers concluded that Raman spectroscopy was effective for differentiating between fresh and spoiled meat. However, it is critical to note that the study did not employ any validation or alternative multivariate classification techniques to corroborate the PCA findings. Similar limitations were present in related research (Schmidt et al. 2010; Sowoidnich et al. 2010). Nonetheless, these series of studies set up the foundation to fast evaluate meat spoilage using Raman spectroscopy, which requires further investigation and comprehensive analysis.

A further study used FT-IR and Raman spectroscopies to detect and record spoilage process in chicken meat (Zając et al. 2017). The research entailed storing chicken breast muscle at 22°C over a ten-day period, during which spectral data were collected. The analysis of the spectral information involved deconvoluting the experimental Raman bands into Lorentzian components. The analytical phase consisted of correlating the integral intensities of specific Raman bands with

the presence of free amino acids and protein structures. This correlation followed patterns identified in prior research. The findings led the authors to affirm that both Raman spectroscopy and FTIR are viable for tracking temporal changes attributable to meat spoilage.

In another study, Yang and others investigated the use of Raman spectroscopy to predict beef spoilage in vacuum packaging and modified atmosphere packaging (Yang et al. 2020). Utilizing a partial least squares regression model, the researchers demonstrated the technique's capability to predict total viable counts and concentrations of lactic acid bacteria 21 days post-mortem. Similarly, the output proved that Raman spectroscopy could reflect meat spoilage by indicating the changes in the secondary structure of proteins and amino acid contents. Yet, it is still required to determine the robustness and repeatability of this model with a larger database.

Overall, the application of Raman spectroscopy in determination of meat spoilage has been preliminarily investigated. In order to better detect meat spoilage, enhancement can be made from two ways: one is to further explore the relationship between intensities of Raman bands and the change of chemical compositions during deterioration process, and the other is to apply more advanced calculating algorithms to conduct multivariate statistical analysis with a larger independent dataset.

2.4 Data Analysis of Raman Spectra

Raman spectral data is in a nature of high dimension. This feature benefits the substantial information included in Raman spectra, but also makes it complicated to interpret the details hidden behind Raman peaks. Improvement of computational approach and experimental setups trigger the development of chemometrics. Chemometric technique is a powerful analytical method to extract information and subtle difference from Raman data using knowledge of mathematics, statistics and computer science. However, the difference in Raman spectra is not only delicate, it is also easily masked by artifacts, such as fluorescence background, instrumental

operation, measurement errors or degradation of samples (Brown et al. 2020). Hence, the process of removing those before applying chemometrics is of great importance. Although there is not yet a standardized procedure and it depends on the user's need, the well-recognized workflow for Raman spectroscopic data analysis consists of data pre-processing and chemometric model construction.

2.4.1 Data preprocessing

Due to the presence of unwanted effects in Raman spectral data, it is necessary to suppress and remove those undesired effects to restore the 'clean' Raman signals of interest by doing data cleaning (Bocklitz et al. 2011). The methodology of Raman spectral pre-processing has been established and it is summarized to be a generally accepted workflow, which includes the steps of quality control, cosmic spikes removal, baseline correction, smoothing, spectral truncation, and normalization (Guo et al. 2021a).

Quality control constitutes the preliminary step, aimed at ensuring the integrity of spectral data by eliminating apparent outliers. These outliers typically exhibit characteristics such as severe photodamage, pronounced signal contamination, or an inadequate signal-to-noise ratio. Identification of these outliers can be performed through visual examination or by employing more objective criteria like Hotelling's *t*-squared, Mahalanobis distance or Q residuals to set exclusion thresholds (Penny and Jolliffe 2001). It is vital to substantiate the outlier status of a spectrum with evidence before its removal, thereby preserving the validity of the dataset.

Subsequent to quality control, the removal of cosmic spikes is imperative. These spikes manifest as abrupt and pronounced peaks within Raman spectra, stemming from high-energy cosmic rays interacting with the charge-coupled device (CCD) detector (Ryabchykov et al. 2016). They appear randomly in Raman spectra and would affect the following analysis of data negatively because of their high intensities. To mitigate this, spike detection and correction

procedures are undertaken. Typically, an interpolation technique, utilizing values from the periphery of the affected regions, is implemented to restore the spectral data compromised by cosmic spikes (Gautam et al. 2015).

Baseline correction is a crucial procedure to eliminate the influence from fluorescence background or substrate. It is easy to remove substrate background only through recording Raman spectra of substrate, followed by subtraction. Removing fluorescence background is more complicated since the background would vary, which requires mathematical calculation. Some common methods exploited for baseline correction are briefly summarized here: 1) polynomial fitting based method, which is a widely adopted method due to its simplicity and efficacy (Lieber and Mahadevan-Jansen 2003); 2) differentiation based method focusing on calculating derivatives, often implemented via the Savitzky-Golay algorithm or kernel estimation (Savitzky and Golay 1964; Wand and Jones 1994); 3) asymmetric least squares method, which provides a more refined correction by weighing the residuals differently (He et al. 2014). Given their flexibility, there is no one-size-fits-all solution - each method has its own merits, and the choice often depends on the requirements of subsequent data analysis. Cautions should be taken while selecting the method because unreasonable baseline correction will mask the original Raman spectral features.

Smoothing of Raman spectra is considered discretionary in data analysis, as its benefits are often minimal and may potentially obscure valuable analytical details (Guo et al. 2021a). Then, the last step of Raman spectra preprocessing is spectral truncation and normalization. Spectral truncation is to cut down the wavenumber regions into a specific region of interest that contains substantial spectral features. After that, normalization is the final procedure that can eliminate the influence of intensity fluctuation. The peak that is constant among different spectra can be chosen as reference and scaled to 1.

It's crucial to recognize that the sequence and choice of preprocessing steps are not set in stone but rather contingent on the specific goals of the analysis. These steps can interact with one another, affecting the overall outcome; hence, they should be viewed holistically. To maintain integrity, it is advisable to apply a uniform preprocessing protocol across all spectra within a given dataset.

2.4.2 Model construction

Multivariate statistical analyses are efficient in translating multiple complex Raman spectra into informative results simultaneously for a better interpretation. There are many chemometric models available for selection and application. Even the models to choose vary between different dataset, the three main objectives of multivariate statistical analysis are: 1) data description; 2) classification, discrimination, and clustering; 3) regression and prediction (Gautam et al. 2015). In the context of this thesis, which centers on classification, discrimination, and clustering, subsequent discussions will concentrate on multivariate statistical analyses tailored for classification.

Chemometric models for classification are typically categorized into two main types: unsupervised and supervised methods (Xu et al. 2020). Unsupervised methods are adept at identifying inherent groupings within an unlabeled data set without prior knowledge of class labels, often serving as a preliminary step to supervised analysis. Principal component analysis (PCA), K-Means clustering, and hierarchical cluster analysis (HCA) stand as exemplary unsupervised techniques (Byrne et al. 2016).

Different from unsupervised methods, supervised methods require to label each class that needs to be discriminated, which can usually achieve a better clustering performance. To be more specific, there are two steps when conducting supervised models. The first phase is to establish a model using patterns from the training dataset, in which the class assignments are known.

Thereafter, the second phase is to use testing dataset to validate the reliability of the model learned from the first step. Common supervised models used in spectroscopic analysis are linear discrimination analysis (LDA), support vector machine (SVM), partial least square discrimination analysis (PLS-DA), Bayes classifier, and decision tree (DT) (Xu et al. 2020). However, these conventional models may not always be sufficient, especially when the underlying relationships in Raman spectral data are intricate. In such instances, advanced machine learning algorithms like artificial neural networks (ANN) can offer substantial improvements in discriminatory power (Özbalci et al. 2013).

While supervised models are potent, their reliance on labeled data can become a challenge, particularly with extensive datasets. Consequently, a hybrid approach that combines unsupervised and supervised methods is sometimes preferable. The subsequent section will provide a succinct overview of various unsupervised and supervised chemometric models that have been implemented in this thesis.

2.4.2.1 Principal component analysis (PCA)

Principal component analysis is one of the best-known unsupervised multivariate statistical analysis technique, which aims to reduce the dimensionality of the data and generate a new set of orthogonal variables called principal components (PCs) (Ilie et al. 2017). The construction of PCs involves the computation of eigenvectors and eigenvalues from the covariance matrix of the data. The first PC captures the greatest variance within the data, with each successive component accounting for the next highest variance. Often, the cumulative variance described by the initial PCs is sufficient to represent the major spectral differences. Consequently, classification of Raman spectra in most cases can be achieved with these first few PCs (Tu and Chang 2012). Further insights can be gleaned from the loadings of the PCs, which elucidate the specific spectral features contributing to the variance (Shinzawa et al. 2009).

2.4.2.2 Logistic regression (LR)

Logistic regression is a type of supervised linear regression model, which performs linear weighted calculation on input data to obtain different weights of input variables and results into possibility. Although the logistic regression model itself merely outputs the possibility of a certain class or event taking place and does not perform classification, it can be used as a classifier by choosing a cutoff value as the decision boundary to discriminate different classes. Previously, LR is most used when the variables are binary or dichotomous. It has been currently generalized to do multi-category classification with multinomial logistic regression model (Dreiseitl and Ohno-Machado 2002; Lieber et al. 2009).

2.4.2.3 Decision tree (DT)

The decision tree is a versatile supervised machine learning algorithm that can facilitate both classification and regression tasks. It mirrors the architecture of a tree, with root nodes, branches, and leaf nodes. Within this framework, each leaf node corresponds to a class label outcome, while the branches serve as decision points that evaluate the attributes leading to those labels (Patel and Prajapati 2018). In the realm of multivariate statistical analysis, the decision tree stands out as a robust technique that integrates mathematical and computational methods to categorize and delineate datasets. A salient advantage of the decision tree model lies in its human-like reasoning capabilities, which allow for the simplification and intuitive interpretation of complex Raman spectral data (Li et al. 2022b).

2.4.2.4 Support vector machine (SVM)

Support vector machine (SVM) represents another sophisticated supervised classification model. Its foundational mechanism involves identifying an optimal hyperplane that serves as a decisive boundary to distinguish between various classes in a dataset (Qi et al. 2023). This optimal hyperplane is constructed by calculating the distance from data points to the boundary and

determine the one that has the maximum margin between separated classes (Lussier et al. 2020). When a new observation is projected into this hyperplane, it can be easily grouped. Sometimes, to handle more complex differentiation mission in higher dimensions, core function will be acquired as a competent technique (Pan et al. 2022). Given its distinctive effectiveness with spectroscopic data, SVM has been extensively applied alongside Raman spectroscopy within the food industry for tasks such as detecting adulteration, conducting compositional assessments, and identifying bacterial strains (Tan et al. 2019; Kelis Cardoso and Poppi 2021; Du et al. 2022).

2.4.2.5 Convolutional neural networks (CNNs)

Convolutional neural networks (CNNs) is a supervised deep machine learning model that is well-known for its ability of feature extraction from images and text (Fukuhara et al. 2019). Recently, CNNs has been employed to classify samples characterized by Raman spectroscopy, and it was reported that CNNs classifiers outperformed other conventional classification methods with a higher accuracy (Kazemzadeh et al. 2022). Some studies used the collected Raman spectra combined with CNNs to differentiate biological samples, such as *E. coli*, pork skin samples, as well as breast cancer tissue (Ho et al. 2019; Sohn et al. 2020; Ma et al. 2021). In addition, CNNs model has the advantage of working as an end-to-end tool, which can analyze spectroscopic data from preprocessing directly to the final classification output (Liu et al. 2017). Such an end-to-end tool can offer an alternative to the conventional analysis pipeline. Hence, the procedure such as baseline correction can be automatically achieved by using the CNNs system.

The computational structure of CNNs mimics the complicated mechanism of how cells in human brain identify and deal with visual images. As shown in **Figure 2.2**, the architecture of CNNs model consists of five parts: input layers, convolutional layers, pooling layers, then followed by fully connected layers and output layers. Raw data can be imported directly into the input layers. Convolutional layers with kernel then will perform to extract features from input

layer, and different kernels extract different features (Gu et al. 2019). Thereafter, the function of pooling layer is to do a second extraction from convolutional layer, which can find out the most prominent characteristic (Liu et al. 2017). Normally, a CNNs architecture contains at least two convolutional layers and two pooling layers. With more layers are set, it is more likely to achieve better clustering results. The fully connected layers act to integrate and connect all the extracted features together to yield a categorization result in the output layers. With well-trained CNNs model, the raw data of Raman spectra can be input and processed to output a certain classification with a high accuracy.

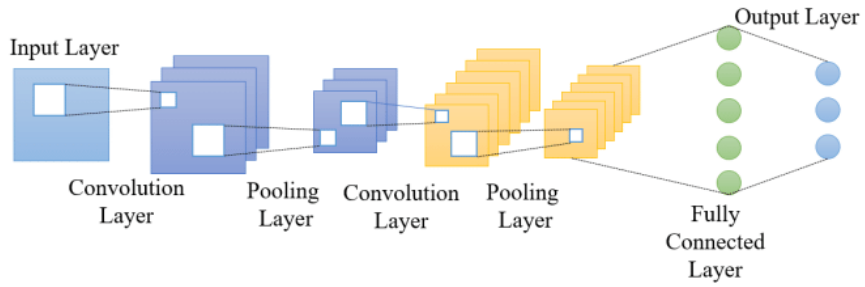

Figure 2.2 Illustration of basic structure of CNNs model (Gu et al. 2019).

2.5 16S rRNA high-throughput sequencing

In this thesis project, the change of features in Raman spectra during pork spoilage process is not only identified by chemometrics but also analyzed by 16S rRNA high-throughput sequencing in parallel to assess how microbial changes can affect Raman spectra. Therefore, the following session will give an introduction of 16S rRNA high-throughput sequencing technique and briefly summarize its application in bacterial community analysis in meat samples.

2.5.1 Mechanism

16S rRNA sequencing has been a powerful technology to clarify the phylogeny and taxonomy of bacteria and archaea in a diverse microbial population (Janda and Abbott 2007). The reasons of wide application of 16S rRNA sequencing for taxonomic classification can be

summarized as: 1) it is available in almost all bacteria. 2) the function and structure of 16s rRNA gene has not changed over time. 3) the length of the 16S rRNA gene can provide enough bioinformation (Janda and Abbott 2007). In general, 16S rRNA is a part of the 30S subunit of prokaryotic ribosome and it binds with 19 proteins to form the structure of the subunit (Schluenzen et al. 2000). To be more specific, 16S rRNA is approximately 1500 base pairs long and includes several highly conserved regions and 9 hypervariable regions that alternate each other (Bukin et al. 2019). The conserved regions can be used to design primers, and the hypervariable regions are for taxonomic classification (Yang et al. 2016). The taxonomic classification is based on the similarity of the hypervariable regions to generate operational taxonomic unit (OTU) by comparing OTU sequence with the database reference. Nowadays, the generally accepted assumption of OTU identification is that more than 95% similarity represents the same genus and more than 97% similarity can be regarded as the same species (Johnson et al. 2019).

Traditionally, 16S rRNA sequencing has been employed with Sanger capillary sequencing to distinguish genus, but this method is low-throughput and the process is time-consuming. The development of next-generation sequencing (NGS) can provide a higher throughput data and enables microbiome analysis based on 16S rRNA.

Next generation sequencing, also known as high-throughput sequencing, is a technique that can sequence nucleotides faster and easier than Sanger sequencing, which is known as first generation sequencing. Compared with the first-generation sequencing, NGS has the improvement of easier preparation and processing millions of sequencing in parallel at the same time. In addition, the detection of bases is performed cyclically and the cost is more effective (Park and Kim 2016). However, current NGS technology rely on much shorter reads and have an intrinsically higher error rate than Sanger sequencing. The likelihood of error that happens vary

among each platform and sequencing scheme so that the users need to be aware of the risks to circumvent these issues. Nowadays, there are lots of available sequencing platforms, such as Roche, Life Technologies, and Illumina, all of which rely on different principles and can fit the need of varied read lengths (Janda and Abbott 2007). Since Illumina platform was used to proceed part of 16S rRNA sequencing in this thesis project, the next paragraph will briefly introduce the mechanism and workflow of Illumina technology.

Illumina workflow includes four basic steps: library preparation, cluster generation, sequencing and data analysis. The first step of library preparation is finished by randomly fragmentating either DNA or cDNA sample, followed by oligonucleotides adapter ligation and adding barcodes. These adapters carry specific sequence and can enable the subsequent amplification and sequencing steps (Modi et al. 2021). For cluster generation, the library will be loaded into a flow cell and the adapters in fragments will be bounded to the complimentary oligos inside the lawn. Through the process of 'bridge PCR', each fragment will be amplified into clusters. Then, those clusters are ready for the sequencing step. While sequencing, Illumina uses reversible terminator-based method that can detect single base and carries out the 'sequencing by synthesis' technology. During each sequencing cycle, the result can be detected by the fluorescent emission of each cluster. Finally, the raw data will be preprocessed into clean data that can be used for downstream analysis. Then, the reads can be aligned to the reference database with specific pipelines.

The high-throughput, effective and accurate attributes made the next generation sequencing based on 16S rRNA an outstanding method to analyze the community compositions and dynamics of microorganisms.

2.5.2 Application in pork spoilage

16S rRNA high-throughput sequencing is recognized as a robust methodology for delineating the complexities of bacterial populations and elucidating the link between microbial shifts and pork spoilage. Various studies have delved into the transformation of microbial community compositions during the spoilage process of pork (Li et al. 2019; Zhou et al. 2020; Zhao et al. 2022b). One such study by Li and colleagues leveraged the V3-V4 hypervariable regions of 16S rRNA for high-throughput sequencing, providing insights into the bacterial communities present in refrigerated pork over a period of ten days (Li et al. 2019). The bacterial diversity decreased as storage time passed, and *Pseudomonas*, *Acinetobacter* and *Photobacterium* were dominant genus in pork samples and closely associated with pork spoilage. Another study used the same technique to analyze how temperature affected the bacterial communities in pork meat (Zhao et al. 2022b). The bacterial compositions were highly similar between pork meat stored at -2°C and 4°C, with *Pseudomonads* and *Brochothrix* being the dominant taxa. In another study, Zhou and others assessed the influence of bacterial extraction methods on bacterial communities of chilled pork (Zhou et al. 2020). The difference in operation led to various profiles of bacteria in the samples, but *Pseudomonas* and *Photobacterium* were present most frequently.

In summary, the composition of bacterial communities in pork is influenced by a myriad of factors, including the origin of the sample, storage temperature, and handling methods. Investigating the microbial profiles throughout the pork spoilage process not only enriches our understanding of potential microbial transitions but also sheds light on the metabolic activities that contribute to spoilage. This knowledge can be leveraged to reinterpret changes in Raman spectra associated with spoilage, potentially unveiling correlations that enhance our ability to monitor and assess meat quality through spectroscopic techniques.

CHAPTER 3. MATERIALS AND METHODS

3.1 Materials

Fresh pork samples of two different portions, namely *musculus semimembranosus* (SM) (~1.5 kg/piece) and tenderloin (~900 g/piece), were supplied from a local company in Montreal. The samples were delivered with vacuum packaging at 4°C in foam box. There were three batches of each portion in total, which were considered as biological replicates. Therefore, each of these two portions had three replicates. Tryptic soy agar (TSA) and phosphate-buffer saline (PBS) were purchased from Sigma-Aldrich (Sigma-Aldrich, Canada). Raman spectra were collected by using an EZRaman-I Series portable Raman spectrometer (Enwave Optronics, Inc., Irvine, CA, USA). The total genomic DNA was extracted by using the DNeasy PowerSoil Pro Kit (Qiagen, Valencia, CA, USA).

3.2 Sample preparation

After the samples were received, each piece of pork meat was split into halves. One half was cut into 9 small pieces, with each weighted 25 g, and then these small cubes were preserved in sterile polyethylene sampling bags (Nasco B01385WA Whirl-Pak® Homogenizer Blender Filter Bags) separately for microbial testing. Another half was cut into 9 pieces of 1 cm thickness and also preserved in sampling bags individually for Raman spectral collection. All these meat samples were stored at 4°C for up to 14 days.

3.3 Microbial testing of pork spoilage

Microbial testing was conducted through two parts simultaneously, namely using the traditional method to detect total viable counts and 16S rRNA high-throughput sequencing. The experiment was conducted on Day 1, Day 2, Day 3, Day 4, Day 6, Day 8, Day 10, Day 12, and Day 14.

3.3.1 Determination of total viable counts

For the determination of total viable counts, a piece of 25 g sample was taken out and 225 mL PBS solution was added, followed by homogenization in a stomacher for 2 min at 22°C. After serial dilutions, 100 μL of the diluted samples was spread onto TSA, followed by incubation at 37°C for 48 h to determine total viable counts. Each sample was analyzed in triplicates.

3.3.2 16S rRNA high-throughput sequencing

3.3.2.1 DNA extraction

Samples of Day 1, Day 4, Day 8, and Day 14 were chosen for DNA extraction and high-throughput sequencing analysis, and each sample was tested in duplicates. On each day, 40 mL of the homogenized solution was centrifuged at 15,000 ×*g* for 5 min. Then, the supernatant was discarded and the pellet was harvested for DNA extraction. Total genomic bacterial DNA was extracted using the DNeasy PowerSoil Pro Kit according to the manufacture's protocols. The DNA quality was confirmed by 1% agarose gel electrophoresis, and the DNA concentration and purity were determined by using a UV-Vis spectrophotometer (NANODROP 2000C, Thermo, USA).

3.3.2.2 High-throughput sequencing

Extracted DNA samples were then sent to Novogene Corp. (Novogene, Beijing, China) for 16S rRNA amplicon sequencing. The V4 variable region of the 16S ribosomal DNA gene was amplified with the primers 515F (GTGCCAGCMGCCGCGGTAA) and 806R (GGACTACHVGGGTWTCTAAT). PCR reactions were carried out with 15 μL of Phusion® High -Fidelity PCR Master Mix (New England Biolabs), 2 μM of forward and reverse primers, and about 10 ng template DNA. Thermal cycling consisted of initial denaturation at 98°C for 1 min, followed by 30 cycles of denaturation at 98°C for 10 s, annealing at 50°C for 30 s, and elongation at 72°C for 30 s, and 72°C for 5 min finally.

The amplified PCR products were mixed with 1X loading buffer (contained SYB green) and detected by 2% agarose gel electrophoresis. Then, the mixture PCR products was purified using the Qiagen Gel Extraction Kit (Qiagen, Germany).

Sequencing libraries were generated using the TruSeq® DNA PCR-Free Sample Preparation Kit (Illumina, USA) following manufacturer's recommendations and index codes were added. The library quality was assessed on the Qubit@ 2.0 Fluorometer (Thermo Scientific) and Agilent Bioanalyzer 2100 system. At last, the library was sequenced on an Illumina NovaSeq 6000 platform (Illumina, San Diego, CA, USA) and 250 bp paired-end reads were generated.

3.3.2.3 Data analysis

The sequencing raw data with primer and barcode removed was trimmed and aligned to obtain high quality sequencing data using mothur v1.48.0 software (https://github.com/mothur/mothur/releases/tag/v1.48.0) following the protocol provided in a previous study (Kozich et al. 2013). Then, the effective tags with 97% similarity were clustered into OTU. Each OTU was assigned to a taxonomy based on SILVA Database (https://www.arb-silva.de/) by a naive Bayesian model using Ribosomal Database Project (RDP) classifier v2.2 (Wang et al. 2007; Quast et al. 2013).

To evaluate richness and diversity of bacterial communities within sample, alpha-diversity indexes including Coverage, Chao 1, ACE, Shannon index, and Simpson's index were calculated (Kemp and Aller 2004). Analysis of variance (ANOVA) was carried out for data analysis, and one-way multiple comparison test by Fisher Least Significant Difference (LSD) test was performed. A *P*-value of < 0.05 was considered as significant. Beta-diversity analysis was performed by Principal Co-ordinate Analysis (PCoA) to evaluate the difference in bacterial composition between samples. All the analyses were conducted using RStudio (http://www.rstudio.org/).

3.4 Raman spectral collection

Raman spectral collection time-points were consistent with microbial testing days, which were on Day 1, Day 2, Day 3, Day 4, Day 6, Day 8, Day 10, Day 12, and Day 14. On each measurement day, sample would be taken out from the sampling bag and deposited onto a clean petri dish covered with polyethylene cling wrap to mimic the pork packaging sold in the supermarket. For each sample, 30 spectra were collected with packaging from 30 different positions. Similarly, 30 spectra were also collected without cling wrap packaging from 30 positions. The portable Raman spectrometer system is equipped with a 785-nm diode laser with a maximum laser power of 282 mW. The Raman scattering signals were generated by illuminating pork samples using a 250-mW laser power over 40-s integration time. The Raman signals over the wavenumber range of 2189-100 cm^{-1} were recorded with signal resolution of 1 cm^{-1}.

3.4.1 Pre-processing of Raman spectral data

First, cosmic spikes were visually inspected and removed from the collected Raman spectral data using NGSLabSpec software (Horiba Jobin Yvon, Edison, NJ, USA). Then, the baseline was corrected by Asymmetric Least Squares Smoothing Baseline method using OriginPro 2021b (OriginLab Corp.) with parameters set as: asymmetric factor = 0.001, threshold = 0.01, smoothing factor = 5, number of iterations = 10. All spectra were normalized to the intensity of the Raman peak at 1002 cm^{-1}, which is attributed to the presence of phenylalanine (Talari et al. 2015).

3.4.2 Spectral analysis using chemometrics

After pre-processing, Raman spectra with the wavenumber region of 960 to 1800 cm^{-1} were used for constructing chemometrics. To identify the spectral features first, Raman spectra of different storage days were analyzed by using PCA and scores plot of the first two PCs were drawn to show the relationships of these profiles using OriginPro 2021b (OriginLab Corp.).

Meanwhile, we tested and compared various supervised classification tools for their abilities to discriminate fresh and spoiled pork meat using Raman spectral information. These tools included logistic regression (LR), decision tree (DT), support vector machine (SVM), and deep learning algorithms based on convolutional neural networks (CNNs). To assess the reliability of these models, we randomly selected 90% of the Raman spectral data as the training dataset, while the remaining 10% was used as testing dataset. During the model training, only the training dataset was visible for the construction and modification of algorithms. The testing dataset was then employed to validate the generalization ability of the models. Four mainstream indexes including accuracy, precision, recall, and F1 score were calculated to evaluate the performance of these classification models (Chen 2021). All the machine learning models were implemented using Python 3.10 and Ubuntu 22.04. For the traditional classification methods such as LR, DT and SVM, they were established by scikit-learn library v1.2.1. The realization of our self-designed neural network was built based on TensorFlow 2.11.

Our self-designed neural network utilizes a one-dimensional CNN as the initial feature extractor from the input Raman spectra tensor. The input tensor has a shape of 1×841, representing intensity information for various frequencies. Subsequently, three convolutional layers and multiple Batch Normalization (BN) layers are employed after the input layer to extract features from the Raman spectral data. Following each BN layer is a ReLu activation (Fuentes et al. 2023). Finally, these features are connected to Fully Connected layers for prediction after passing through a Global Average Pooling layer and a Flatten layer.

CHAPTER 4. RESULTS AND DISCUSSION

4.1 Determination of microbial growth curve

Microbial analysis is the most traditional and generally applied method used to detect bacterial levels. In this study, we firstly determined the total viable counts (TVC) of microorganisms on pork samples during the storage period. **Figure 4.1** displays the examined microbial growth curve for both pork tenderloin [**Figure 4.1** (a)] and pork *musculus semimembranosus* (SM) [**Figure 4.1** (b)]. The TVC of each sample increased during refrigerated storage. In the case of both pork tenderloin and pork SM, the TVC curve pointed out an initial lag phase from day 1 to day 2. After this time slot, bacteria grew exponentially until day 8, and then entered the steady state with microbial loads between 10^9 and 10^{10} CFU/g, indicating the complete spoilage of meat samples. According to China national food safety standard (GB/T 9959.2–2008), the upper tolerable limit of microorganism in fresh and frozen pork is 10^6 CFU/g. The dashed lines in the figure indicate the threshold value of 10^6 CFU/g. For the two different portions, day 4 is the threshold time point where the TVC values of days before day 4 (including day 4) are below 10^6 CFU/g, and TVC values exceeded this upper limit after day 4. Therefore, pork samples of day 1-4 could be classified as fresh, and the pork meat after day 4 could be regarded as spoilage. Furthermore, the TVC values differed slightly between samples, and this could be explained by the inhomogeneity nature of the meat samples and complicated components of each batch, such as the content of fats, proteins and carbohydrates.

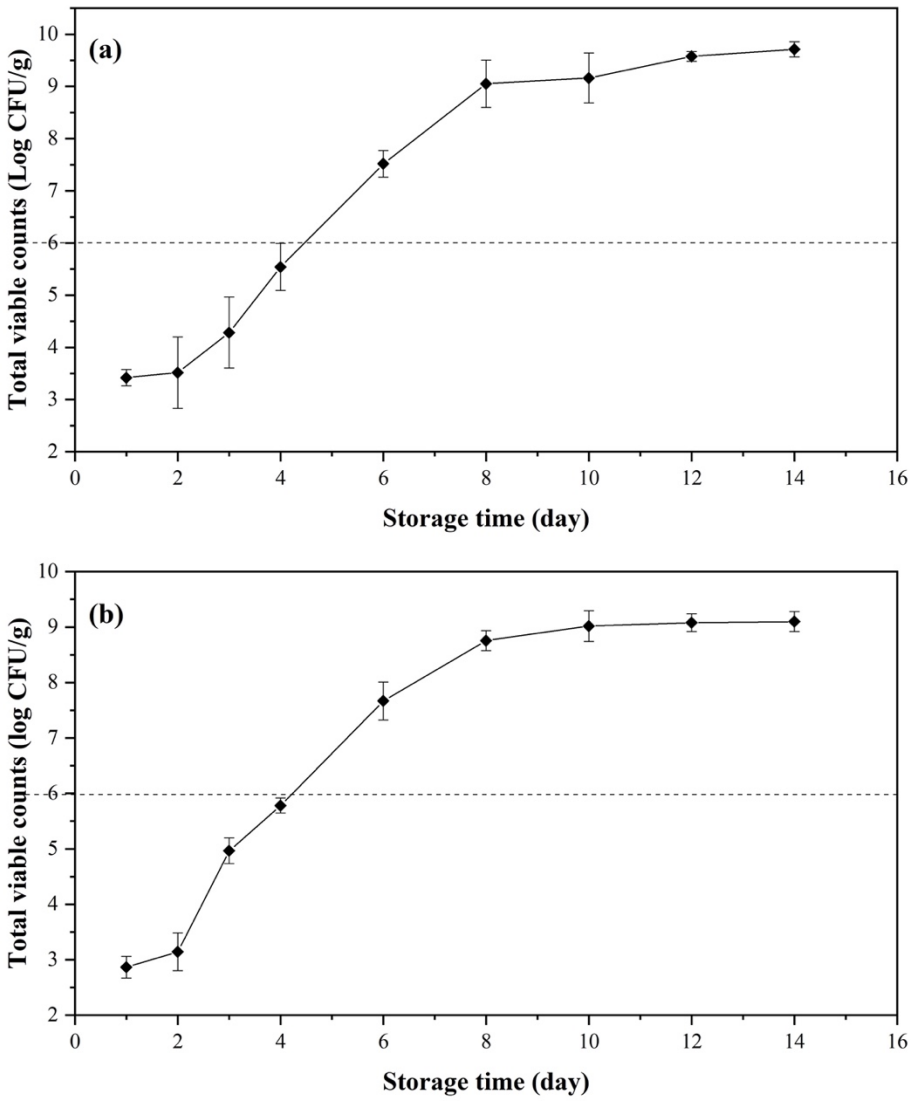

Figure 4.1 Total viable counts (TVC) of (a) pork tenderloin and (b) pork *musculus semimembranosus* (SM). The dashed lines indicate the threshold value of 10^6 CFU/g.

4.2 Raman spectroscopic analysis

4.2.1 Raman spectra of pork tenderloin (TL)

Storage time-dependent Raman spectra with the labels of characteristic Raman bands of pork tenderloin (TL) in the wavenumbers of 960-1800 cm^{-1} are presented in **Figure 4.2**. Raman spectra of **Figure 4.2** (a) are collected without packaging, and Raman spectra of **Figure 4.2** (b) are collected with packaging. For clarity, the spectra are baseline corrected, normalized and

averaged. In accordance with the result of TVC test, Raman spectra of day 1, 2, 3, 4 are classified as 'fresh', and shown in green lines. Meanwhile, spectra of day 6, 8, 10, 12, 14 are regarded as 'spoiled' and matched with red lines. To demonstrate the difference in time slot within each class (fresh or spoiled), the darker color means a longer storage time. In addition, some characteristic Raman bands observed in the spectra and their tentative assignments are summarized in **Table 4.1**.

As shown in **Figure 4.2**, in line with the storage time, the Raman spectra generally maintain their basic shapes, but some major peaks change gradually. The pork TL sample show typical protein spectra where Raman bands for amide I at 1653 cm^{-1}, amide II at 1080 cm^{-1}, and amide III at 1268 and 1318 cm^{-1} could be observed (Movasaghi et al. 2007; Sowoidnich et al. 2012). These protein-related bands are crucial as they can reflect the secondary structures information of proteins in meat sample, thus they are important indicators of meat spoilage. Specifically, amide I and amide III are considered to be more structure-sensitive than amide II (Chi et al. 1998; Talaikis et al. 2020). Therefore, amide I and amide III are mainly chosen as the markers for the analysis of protein structure and content. From the results of Raman spectra, some conclusions could be drawn on the mechanism of meat spoilage. As mentioned before, the progress of pork meat spoilage is accompanied by the degradation of proteins. The content of proteins decreased during spoilage, which could be clearly observed from the decreased intensities of the bands at 1653 cm^{-1}, 1318 cm^{-1} and 1268 cm^{-1}, which correspond to amide I and amide III. It can be seen from the spectra that even at the early stage of the storage, slight changes of protein spectra still occurred. This results was consistent with other previous studies that amide I and amide III would decrease during storage as the result of protein breakdown and the disordered arrangement of protein secondary structures (Zając et al. 2017; Jaafreh et al. 2018; Yang et al. 2020). This was

closely related to the increase in the number of TVC during storage and decomposition of proteins by bacteria.

Moreover, the sharp and strong peak at 1002 cm^{-1} is exhibited by aromatic ring containing amino acids (Zhu et al. 2011). This band is attributed to phenylalanine, which is stable to the environmental changes (De Gelder et al. 2007). The phenyl ring can preserve its amount in the proteins even after protein hydrolysis, indicating that the change in phenylalanine cannot be reflected by the differences in Raman spectral intensity at 1002 cm^{-1} and this peak cannot be utilized for determining pork spoilage. Consequently, this band can be used as a standardized reference point when the Raman spectra are normalized (Nawrocka et al. 2016).

Tyrosine (Tyr), also an aromatic amino acid, is characterized in the Raman spectra at 1176 and 1206 cm^{-1}. Pork is high in dietary tyrosine, and tyrosine is present in a variety of proteins (Kühn et al. 2019). The degree of autolysis and bacterial spoilage have been estimated by detecting tyrosine in some previous studies (Strange et al. 1977). Due to the growth of bacteria and proteolysis of pork meat, extra free tyrosine may be produced, which should be reflected on the Raman signal intensity of Tyr bands. Although this trend was observed slightly opposite in our results for both **Figure 4.2** (a) and **Figure 4.2** (b), the intensities of Tyr bands did not significantly vary. This may be explained by spectral variation or decarboxylation reactions of Tyr and formation of biogenic amine tyramine (Triki et al. 2018). Similar to Tyr, tryptophan (Trp) at 1552 and 1618 cm^{-1} were also clearly identified. There was no obvious difference in the intensity of Raman bands at 1552 cm^{-1}, and the intensity of bands at 1618 cm^{-1} became weaker during the storage. This phenomenon may be induced by the conversion of tryptophan into indole, which is an important indicator of protein decomposition in pork caused by bacteria metabolism. Furthermore, characteristic bands of residues and protein backbone [C-C stretch (νCC) and C-N stretch (νCN)] at 1053 and 1080 cm^{-1} were also notable in the spectra (Sowoidnich et al. 2012).

Comparing the Raman spectral results collected without polyethylene cling wrap packaging [**Figure 4.2** (a)] and with packaging [**Figure 4.2** (b)], the shapes and peaks from two figures were similar, and the Raman peaks generated from polyethylene wrapper could not be observed. This might be due to the fact that one-layer packaging of cling wrap is thin that mimics the actual packaging commonly used in the grocery stores and the laser of Raman spectroscopy focused directly on the meat surface passing through the packing material. This outcome denotes that Raman device has the potential to be used in actual situation for detecting pork spoilage without removing the packaging, which enhances the convenience of the application greatly.

Overall, the Raman spectra show distinguishable capability of recognizing changes of secondary structure of proteins and content of amino acids that can be treated as the indicators of pork spoilage. As the number of microbial colony counts grows, proteolysis happens and the number of free amino acids increases as well. Therefore, the changes of pork compositions can be detected and recorded by Raman spectroscopy during the preservation and spoilage process. However, it is challenging to identify the spoilage levels only via visual examination because of the large amount of data or the subtle difference. To determine more detailed information and achieve rapid detection of pork spoilage, multivariate statistical analysis such as PCA and application of machine learning algorithms are required, which will be discussed in the next section.

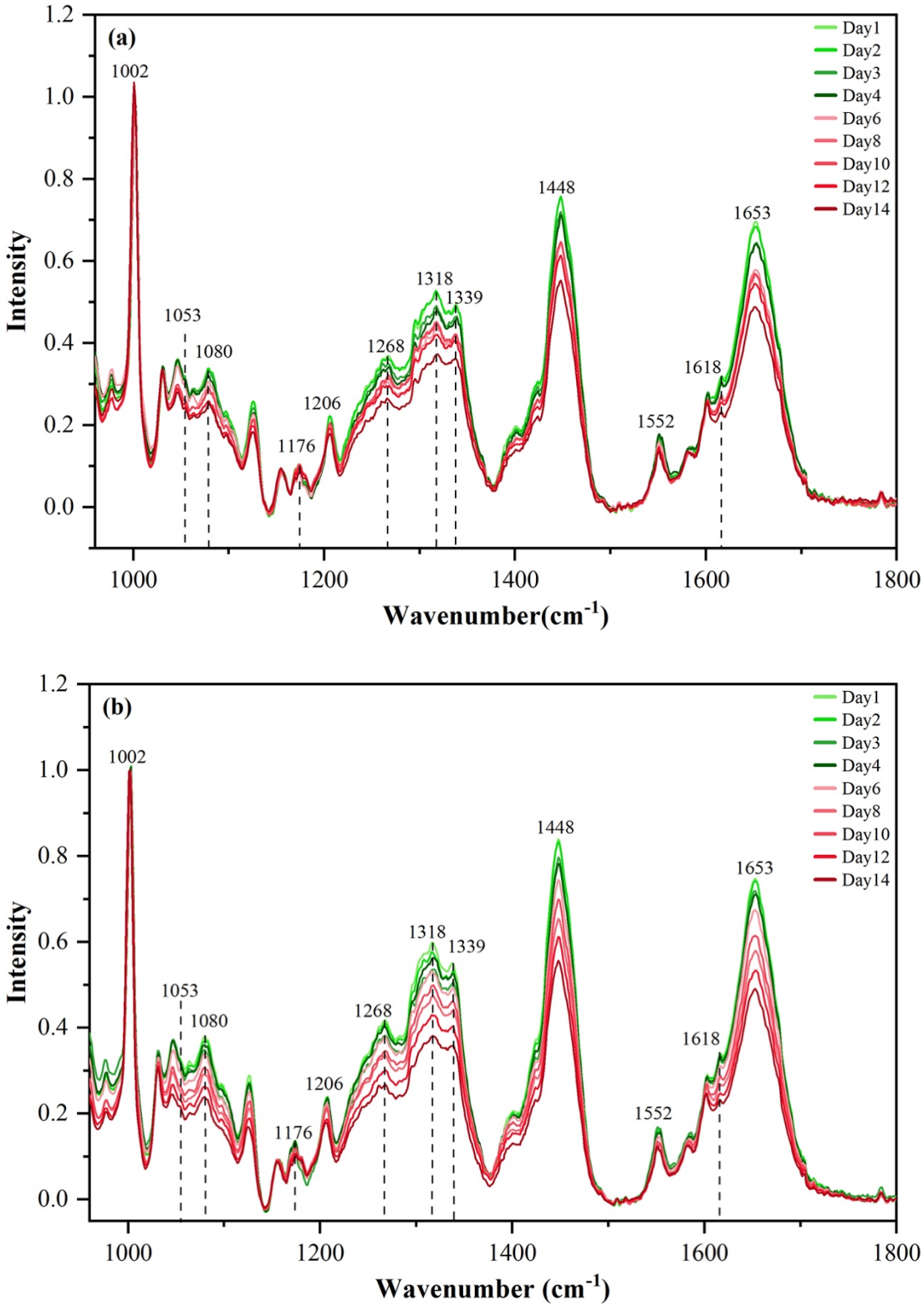

Figure 4.2 Averaged background corrected and normalized Raman spectra of pork tenderloin (TL) in storage time of day 1, 2, 3, 4, 6, 8, 10, 12, and 14. **(a)** Raman spectra collected without packaging. **(b)** Raman spectra collected with packaging.

Table 4.1 Assignments of major peaks in Raman spectra

Wavenumber (cm^{-1})	Peak assignment (Talari et al. 2015)
1002	Phenylalanine
	Phenylalanine (collagen assignment)
1033	Phenylalanine of collagen
1053	C-O stretching, C-N stretching (protein)
1080	Amide II
	Typical phospholipids
	Phosphate vibrations (phosphodiester groups in nucleic acids)
	Tryptophan
1176	C-H bending tyrosine (proteins)
1206	Tyrosine, hydroxyproline
1268	Amide III (collagen assignment)
1318	Amide III (α-helix)
1339	Tryptophan, CH2/CH3 wagging, twisting and/or bending mode of collagens and lipids
1448	CH_2 deformation (protein vibration), a marker for protein concentration
1552	Tryptophan, ν(C=C), porphyrin
1618	Tryptophan, ν(C=C), porphyrin
1653	Amide I, carbonyl stretch (C=O)

4.2.2 Raman spectra of pork *musculus semimembranosus* (SM)

The storage-time dependent Raman spectra of pork *musculus semimembranosus* (SM) stored up to 14 days at 4°C are displayed in **Figure 4.3**. The data are also baseline corrected, normalized to the intensity at 1002 cm^{-1}, and then averaged. As described previously, Raman spectra of pork SM collected without packaging is presented in **Figure 4.3** (a), and spectra collected with packaging is shown in **Figure 4.3** (b). In addition, the colors of lines are

corresponding to the microbial results, where green-like color denotes fresh samples and red-like color denotes spoiled samples.

Similar to the results obtained from pork TL, in the Raman data of pork SM, the decrease of intensities of protein related bands such as amide I and amide III could be observed clearly. In addition, the increase of tyrosine content could be seen from the bands at 1176 cm^{-1}. According to **Figure 4.2** and **Figure 4.3**, the Raman spectra of pork TL and pork SM had the similar spectra shapes and dominant peaks. The trend of how the intensities of Raman bands change in the result of pork SM was consistent with the previous description of pork TL. To avoid repetition, detailed description of those involved peaks could be found in section 4.2.1. To conclude, based on the result of our study, Raman spectroscopy also shows its competency to detect and identify spoilage caused by microorganisms in pork SM samples.

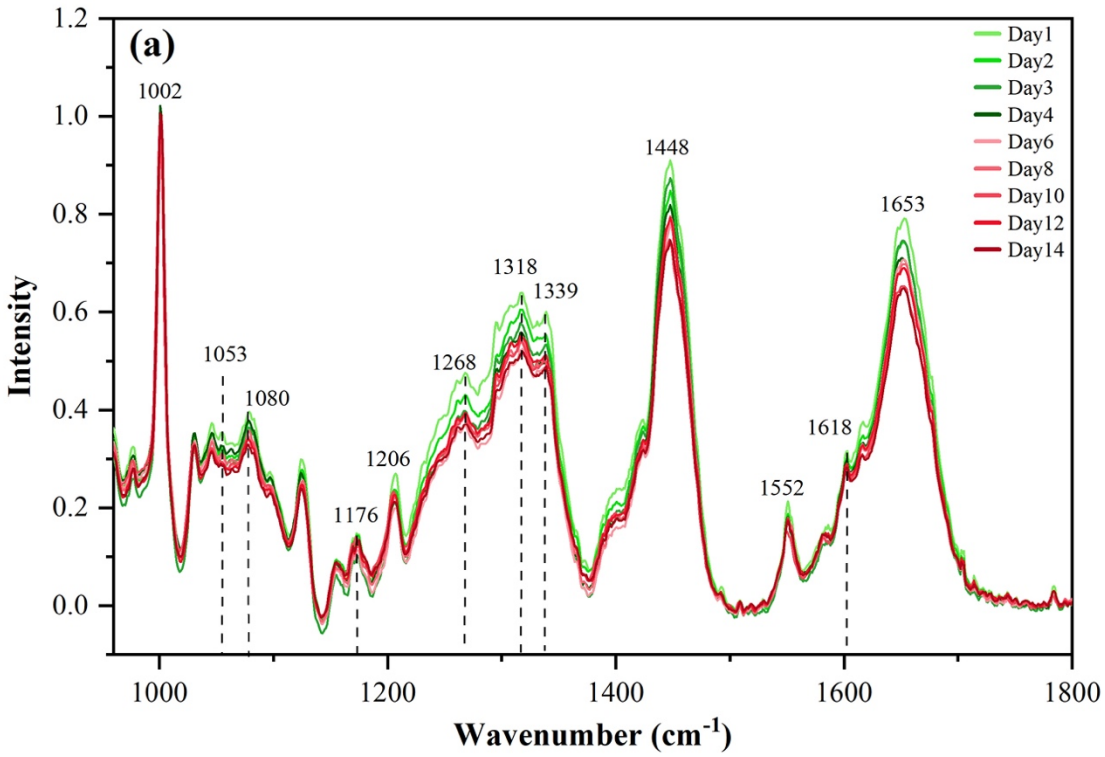

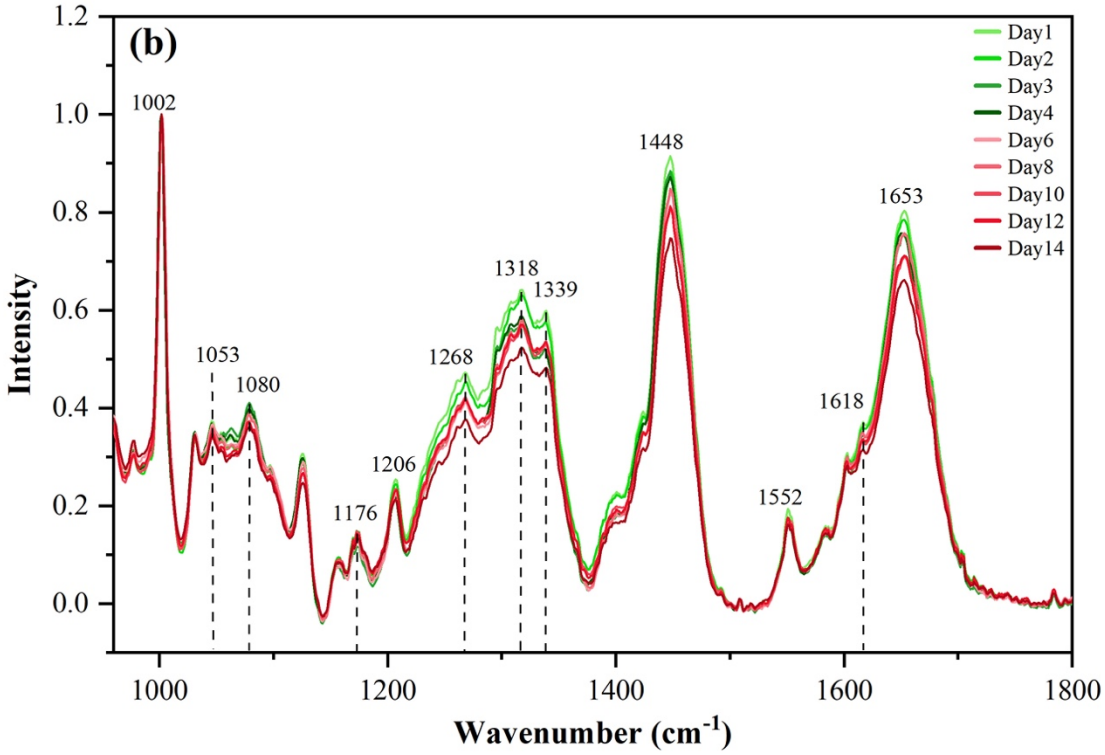

Figure 4.3 Averaged background corrected and normalized Raman spectra of pork *musculus semimembranosus* (SM) in storage time of day 1, 2, 3, 4, 6, 8, 10, 12, and 14. **(a)** Raman spectra collected without packaging. **(b)** Raman spectra collected with packaging.

4.3 Classification of fresh and spoiled pork meat

4.3.1 Principal component analysis

To determine more detailed information of spectral changes, principal component analysis was applied on the preprocessed Raman spectra in the wavenumber region from 960 to 1800 cm^{-1}. Classification of Raman spectra from pork samples are displayed through scores of PCA plots for PC1 and PC2 since these two PCs carry most of the spectral variations between pork samples under different storage times (Brereton 2007). The pork samples could be grouped into two classes, according to the results of microbial analysis, fresh (day 1, 2, 3, 4) shown in green dots and spoilage (day 6, 8, 10, 12, 14, 16) shown in red dots. **Figure 4.4** presents the PCA scores plot from pork TL without packaging [**Figure 4.4** (a)] and with packaging [**Figure 4.4** (b)], and pork SM without packaging [**Figure 4.4** (c)] and with packaging [**Figure 4.4** (d)].

As shown in **Figure 4.4**, i the principal component analysis (PCA) did not reveal a distinct demarcation between fresh and spoiled pork, resulting in overlapping clusters. T This blurring is anticipated because spoilage is a progressive process, and a clear separation between stages is not always evident. Compared with previous studies of using Raman spectroscopy to identify spoilage in poultry or porcine samples, where obvious clustering of different groups of freshness could be observed in the PCA plots, our study increased the number of replicates and robustness of data largely (Sowoidnich et al. 2010, 2012; Jaafreh et al. 2018). Those studies represented each day's readings with daily averaged Raman spectra, which facilitated clear day-to-day clustering in PCA analysis. With respect to our study, all the Raman spectral data collected from three biological replicates at different times were employed for drawing PCA plots. While analyzing Raman spectra within each biological replicate individually, the trend of data dots changing from fresh to spoiled could be observed, which revealed the ability of Raman spectroscopy to detect the variations during pork storage. When combining data received from all the replicates together, this trend disappeared and was replaced by overlapping. This is attributed to the complicated constituents of pork and the heterogeneity among each sample.

Although the categorization of different groups is not significant seen from scores plot of PCA, it is possible to discover the complex spectral changes during pork spoilage. To analyze which Raman bands are responsible for the separation in PCA, plots of PC1 and PC2 loadings are displayed in **Figure 4.5**. Since the loading plots of four PCA results are similar, only the loading plots of pork TL samples (without packaging) is selected to be shown for better illustration and the Raman spectra of the first measurement day was also exhibited for correlating loading scores with the Raman bands. As shown in **Figure 4.5** (b), the main contributors of PC1 were amide III bands at 1268 and 1318 cm^{-1}, amide I band at 1653 cm^{-1}, amide II band at 1080 cm^{-1}, C-O stretching and C-N stretching at 1053 cm^{-1}, tryptophan at 1339 cm^{-1}, and CH_2

deformation at 1448 cm^{-1}. These bands were correlated with a negative sign of loadings, and most of these bands were closely related to the spectra of protein moieties. Except for the bands mentioned above, significant contributors arise for PC2 from phenylalanine of collagen at 1033 cm^{-1}, C-O stretching and C-N stretching at 1053 cm^{-1}, and amide II band at 1080 cm^{-1}. These bands are correlated with a positive sign of loadings. This conclusion is in accordance with the previous studies that the variations of Raman spectra from different storage days were mainly induced by the decomposition of proteins during spoilage process.

The classification ability of fresh and spoiled groups was not satisfactory using PCA due to the inhomogeneity nature between each biological replicate. To perform superior categorization and build a larger database, supervised advanced machine learning algorithms were applied.

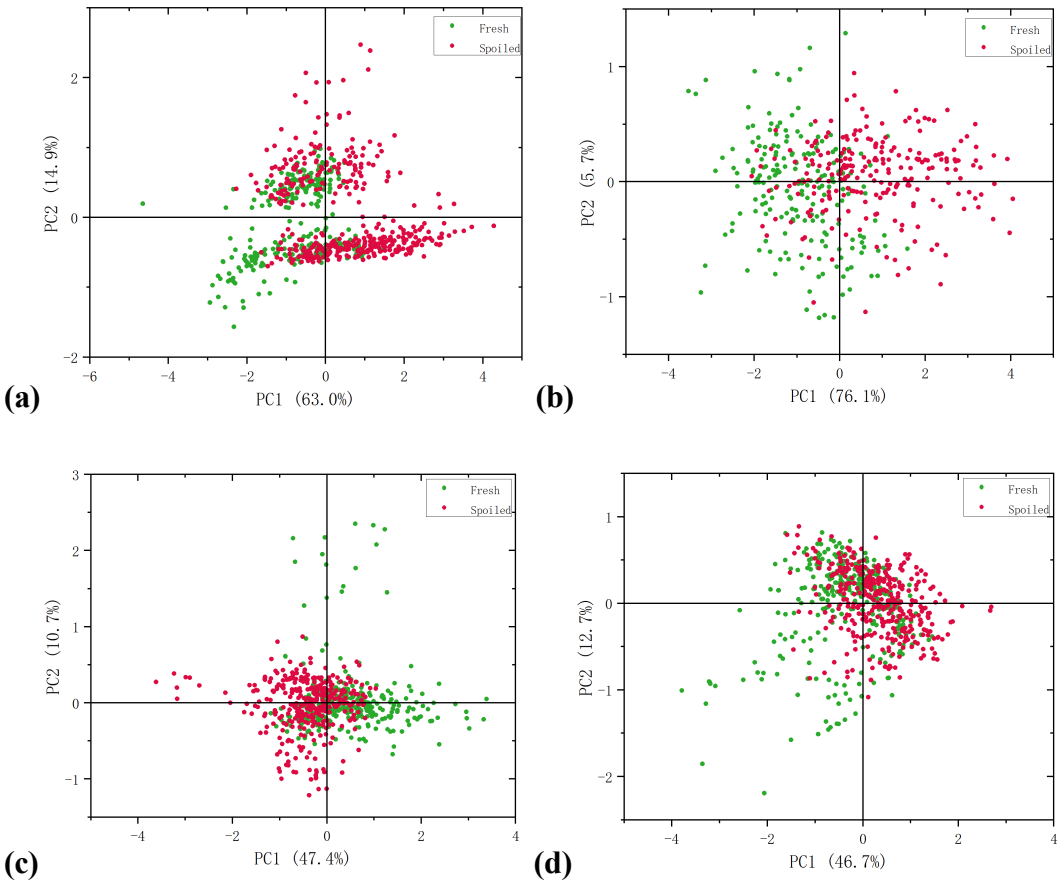

Figure 4.4 Principal component score plots of Raman spectra from: **(a)** pork tenderloin (TL) (without packaging). **(b)** pork tenderloin (TL) (with packaging). **(c)** pork *musculus*

semimembranosus (SM) (without packaging). **(d)** pork *musculus semimembranosus* (SM) (with packaging)

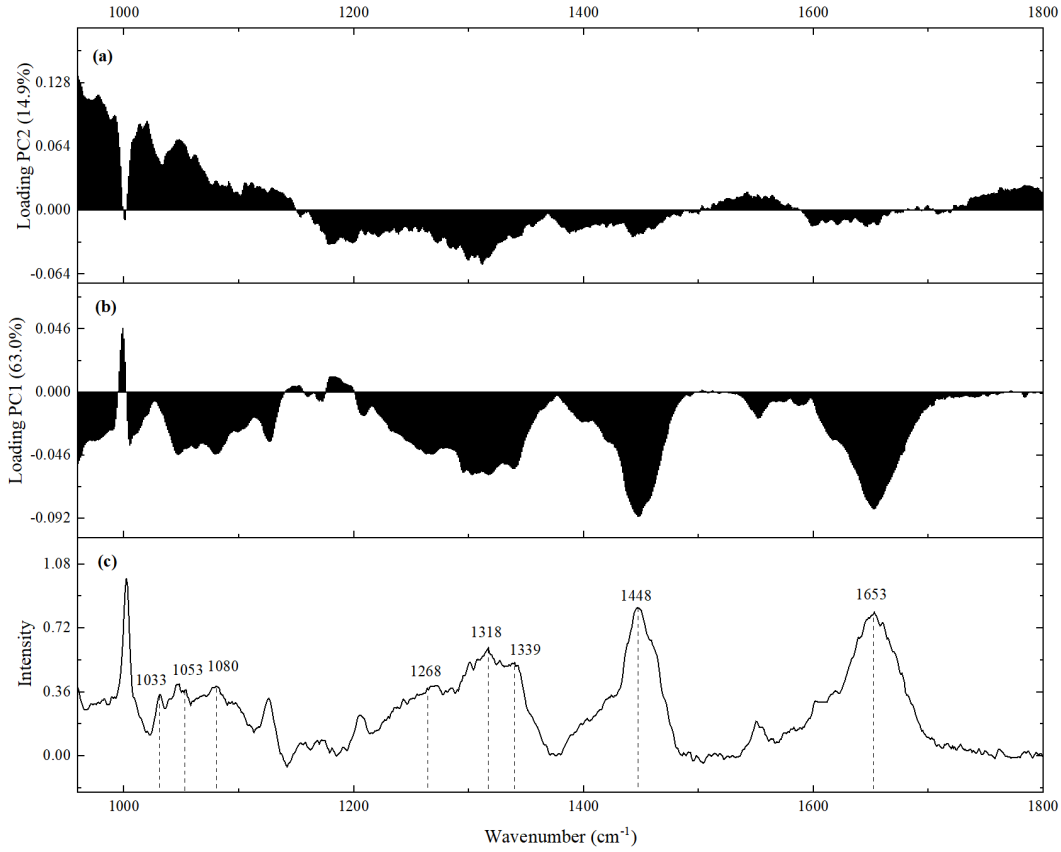

Figure 4.5 Loadings of the PCA of Raman spectral data (pork TL, without packaging) for PC1 **(b)** and PC2 **(a)**. Raman spectra of the first measurement day **(c)** are shown for comparing the Raman bands.

4.3.2 Supervised machine learning algorithms

In order to evaluate the ability of Raman spectra for detecting pork spoilage and also construct a database for future application in food industry, four classification machine learning algorithms were investigated, and their performances are summarized in **Table 4.2** and **Table 4.3**. In the current study, two-class classification for fresh or spoiled recognition of pork TL and pork SM were explored using four models, namely LR, DT, SVM and CNNs. Additionally, four parameters (i.e., accuracy, precision, recall and F1 score) were calculated to assess the

performance of these models (Wang et al. 2021b). Among different types of classifiers, CNNs model with 3 convolutional layers provided >90.00% accuracy, with the highest accuracy of 93.79% when classifying pork TL samples collected with packaging. Meanwhile, LR and SVM models provided the second-best and similar performance for most of the results, with the value of accuracy around 80.00%. However, DT model showed the worst classification ability to discriminate fresh and spoiled samples with identification accuracy ranging from 64.71% to 75.00%.

According to the previous results, Raman spectra from day 1, 2, 3, 4 are labeled as fresh group, and Raman spectra from day 6, 8, 10, 12, 14 are labeled as spoiled, indicating that the number of spectra in the spoiled group is more than fresh group due to the uneven measurement days. Therefore, the dataset is unbalanced as the number of samples in one class is larger than the number of samples in the other class (Chicco and Jurman 2020). Under the circumstances, accuracy may cause misleading result because it would provide overestimation of the classifier ability on the majority class, and this phenomenon is called accuracy paradox (Sokolova et al. 2006; Chicco and Jurman 2020; Alexander et al. 2023). To counteract this, additional performance metrics like precision, recall, and the F1 score must be considered for a comprehensive evaluation of the classification model's efficacy. When assessing these metrics, CNNs model still outperforms others reaching almost more than 90.00% of precision, recall and F1 score. Similarly, SVM and LR models provided results close to 80.00%, and DT model had the lowest precision, recall and F1 score for both pork TL and pork SM samples. These outcomes not only corroborate the proficiency of Raman spectroscopy in distinguishing between fresh and spoiled pork but also highlight the CNN model's superiority in classifying spectroscopic data relative to other established algorithms.

Although pork spoilage can be visually recognized at the later stage of storage, there is a clear need to establish spectral databases and classification models to facilitate high-throughput and automated analysis. This is particularly crucial during the critical transition phase, where subtle shifts in pork's chemical composition are indicative of early spoilage. Studies have illustrated that Raman spectroscopy, when coupled with Convolutional Neural Networks (CNNs), can significantly enhance the accuracy of freshness detection in seafood, such as a reported 90.60% accuracy in classifying the freshness of sea bass fillets, surpassing traditional methods like PCA, PLS-DA, and SVM (Wang et al. 2023). In another study, the authors employed hyperspectral imaging technology coupled with CNN to distinguish fresh and frozen-thawed beef, reaching the accuracy of 88.89% (Pu et al. 2023). Referring to the similar research, the overall accuracy, precision, recall and F1 score of the CNNs model used in our study is satisfactory, and the ability of this CNNs model for identifying pork spoilage is confirmed. To further improve the power of the classifier as well as for the application of Raman spectroscopy-based tool for rapid detection of pork spoilage in real-world scenarios, it is important to increase the number of biological replicates.

Table 4.2 The optimized models for 2-class classification of fresh and spoiled pork tenderloin (TL) samples based on Raman spectral data.

Sample type	Number of spectra	Model	Classification performance			
			Accuracy	Precision	Recall	F1 score
Pork TL (without packaging)	688	LR	77.61%	74.42%	88.89%	0.81
		DT	70.15%	77.14%	69.23%	0.73
		SVM	79.10%	86.49%	78.05%	0.82
		CNNs	91.45%	93.21%	90.68%	0.92
Pork TL (with packaging)	536	LR	79.54%	77.27%	80.95%	0.79
		DT	75.00%	70.37%	86.36%	0.78
		SVM	83.65%	84.18%	87.23%	0.86

	CNNs	93.79%	95.40%	95.62%	0.96

Table 4.3 The optimized models for 2-class classification of fresh and spoiled pork *musculus semimembranosus* (SM) samples based on Raman spectral data.

Sample type	Number of spectra	Model	Classification performance			
			Accuracy	Precision	Recall	F1 score
Pork SM (without packaging)	627	LR	77.27%	75.00%	81.82%	0.78
		DT	69.70%	66.67%	70.97%	0.68
		SVM	80.30%	80.49%	86.84%	0.84
		CNNs	90.44%	91.25%	93.36%	0.93
Pork SM (with packaging)	675	LR	79.41%	78.94%	83.33%	0.81
		DT	64.71%	62.16%	69.70%	0.66
		SVM	76.47%	80.00%	75.68%	0.78
		CNNs	89.92%	88.47%	91.53%	0.90

4.4 Sequencing data analysis

To evaluate the correlation between bacterial composition and Raman spectral changes during spoilage, 16s rRNA high-throughput sequencing of pork samples collected from day 1, 4, 8, and 14 were applied. For sequencing data analysis, bacterial richness and diversity were determined by calculating alpha-diversity including Simpson, Shannon, ACE and Chao 1 indexes, and beta-diversity was analyzed by Principal Co-ordinates Analysis (PCoA). In addition, bacterial community and its dynamics were evaluated based on calculating relative abundance at both phylum and genus levels.

4.4.1 Bacterial richness and diversity

4.4.1.1 Pork tenderloin (TL)

A total of 1,675,007 high quality effective sequences were obtained by merging and filtering raw sequence from each sample, with length from 250 bp to 270 bp. Effective sequences were clustered into 7312 OTUs according to 97% similarity. To form an overall picture, the results of the analysis of averaged alpha-diversity indexes are presented in **Table 4.4**. To better observe

those values, alpha-diversity indexes of each sample are shown in **Figure 4.6**, including **(a)** Chao1 index **(b)** ACE index, **(c)** Shannon index, and **(d)** Simpson 1 index. To explain the meaning of the labels, samples of four measurement days (day 1, 4, 8, and 14) were selected for sequencing analysis because they were critical time points. Day 1 was the beginning of storage, and day 4 represented the end of fresh status. While day 8 was the start of steady status of microbial growth and day 14 was the end of the whole experiment, both representing the spoilage status. There were two batches selected for testing on each measurement day, and each batch included two replicates prepared from two subsamples.

Alpha-diversity metrics summarize the diversity within a single sample, with respect to its richness (number of taxonomic groups present) and diversity (distribution of the abundance of the groups) (Willis 2019). Typically, Chao 1 and ACE (abundance-based coverage estimator) indexes are generated to estimate the total number of species in a community, while Shannon and Simpson indexes are often used to measure the diversity of a community, taking both abundance and relative abundances into account (Xia and Sun 2023). The data presented in **Table 4.4** and **Figure 4.6** reveal a gradual decline in the Chao 1 and ACE indices over the storage duration, with a marked decrease by day 14. Similarly, the Shannon and Simpson indices for days 4, 8, and 14 were substantially lower compared to the baseline established on day 1. This downward trend indicates a diminishing richness and evenness within the bacterial community, reflecting an increase in dominance by particular bacterial species—a finding that aligns with the outcomes of similar research (Li et al. 2019). Additionally, the coverage metrics exceeded 98% across all samples, indicating a comprehensive representation of the predominant microorganisms in the pork TL samples.

Principal Coordinates Analysis (PCoA) was employed to assess beta-diversity, reflecting the variations in species composition among samples at different stages of storage, as visualized

in **Figure 4.7** (Heino et al. 2015). The samples from day 1 were distinctly segregated from those of subsequent days, indicating a significant initial difference in the bacterial community structure of the fresh pork. Conversely, the samples from days 4, 8, and 14 formed a cluster, suggesting that their bacterial compositions became increasingly similar as storage progressed, and the differences between these time points were not substantial.

Table 4.4 The averaged alpha-diversity indexes calculated for the bacterial communities of pork tenderloin (TL) samples for high-throughput sequences reads determined at a 97% similarity.

Attribute	Storage time (days)			
	1	4	8	14
Coverage	0.9846 ± 0.0018^{c}	0.9855 ± 0.0033^{bc}	0.9892 ± 0.0028^{ab}	0.9912 ± 0.0034^{a}
Chao 1	1423.27 ± 166.97^{a}	1310.26 ± 227.37^{a}	1044.16 ± 159.43^{ab}	752.78 ± 296.45^{b}
ACE	1483.37 ± 238.33^{a}	1436.83 ± 217.4^{a}	1136.15 ± 258.14^{ab}	821.86 ± 304.6^{b}
Shannon	3.07 ± 0.51^{a}	1.67 ± 0.61^{b}	1.22 ± 0.39^{b}	1.31 ± 0.87^{b}
Simpson	0.87 ± 0.03^{a}	0.48 ± 0.14^{b}	0.38 ± 0.14^{b}	0.39 ± 0.26^{b}

The data with various upper lowercase letters in each vertical column indicate the significant difference ($P < 0.05$).

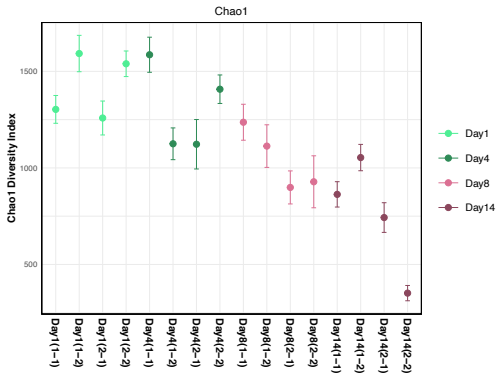

(a)

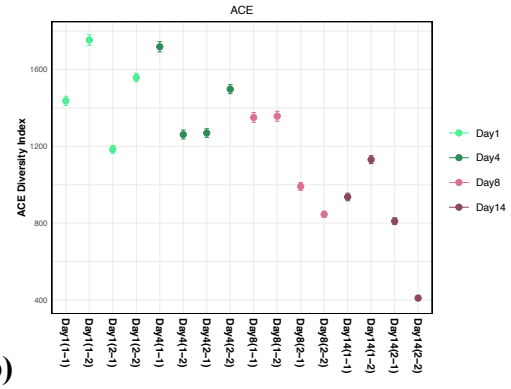

(b)

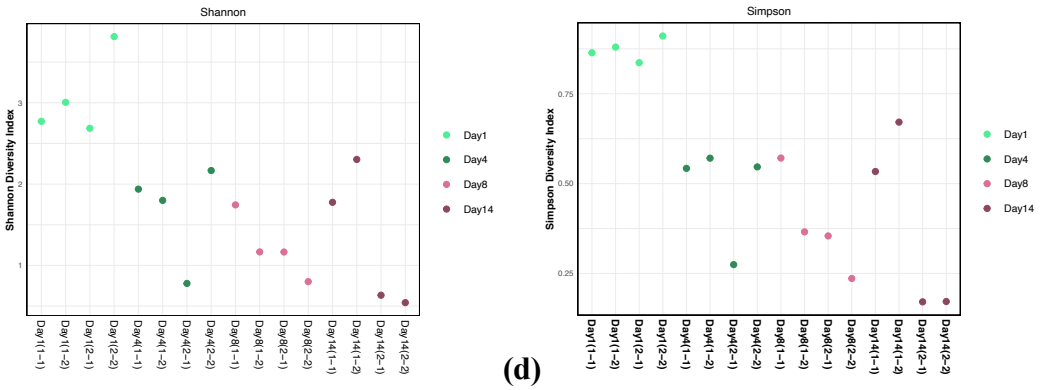

(c) **(d)**

Figure 4.6 Alpha-diversity indexes calculated for the bacterial communities of pork tenderloin (TL) samples for high-throughput sequences reads determined at a 97% similarity. **(a)** Chao1 index. **(b)** ACE index. **(c)** Shannon index. **(d)** Simpson index.

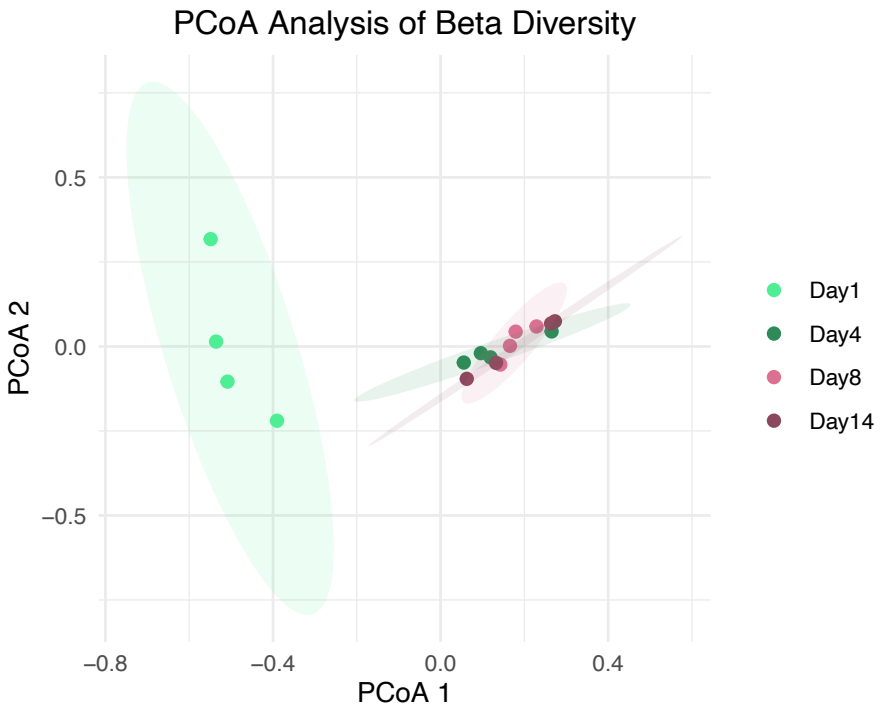

Figure 4.7 Principal co-ordinate analysis (PCoA) of bacterial communities of pork tenderloin (TL) samples.

4.4.1.2 Pork *musculus semimembranosus* (SM)

A total of 1,646,114 high quality effective sequences were obtained by merging and filtering raw sequence from each sample, with length from 250 bp to 270 bp. Effective sequences were

clustered into 5878 OTUs according to 97% similarity. The averaged alpha-diversity indexes of each day are displayed in **Table 4.5**, and the alpha-diversity indexes of each sample are shown in **Figure 4.8**, including **(a)** Chao1 index, **(b)** ACE index, **(c)** Shannon index, and **(d)** Simpson index.

Contrary to expectations, the Chao 1 and ACE indices depicted in **Table 4.5** and **Figure 4.8** showed an increase over the storage period, implying that the number of operational taxonomic units (OTUs) rose with extended storage time. This anomalous trend may be attributed to a multitude of factors, such as the intrinsic inhomogeneity of the pork SM samples, environmental variables, and the potential release of nutrients favoring the proliferation of certain bacteria. Notably, substantial variance within the same batch contributed to a large standard deviation in average values, possibly due to the subsamples being stored separately. Given the significant intra-sample variability, additional replicates might be required to enhance the robustness of these findings. Consistent with previous observations in pork TL and corroborating other studies, the Shannon and Simpson indices were notably reduced by days 4, 8, and 14 compared to day 1, suggesting a decline in microbial evenness as certain bacterial species predominated. The coverage exceeding 99% for all pork SM samples suggests a comprehensive detection of the bacterial community.

The analysis of beta-diversity using Principal Coordinates Analysis (PCoA), as presented in **Figure 4.9**, reinforced the trends observed in pork tenderloin (TL) samples. On the initial day, the freshest pork SM samples were clearly delineated from those of later dates, with no overlaps evident. This clear segregation on day 1 underscores a distinct bacterial community composition at the outset of storage. As storage time progressed, the samples from days 4, 8, and 14 grouped closely, suggesting a convergence in microbial composition across these times. This pattern of beta-diversity for pork SM samples corroborates the findings from the pork TL sample set, affirming the consistency of the microbial dynamics regardless of the cut of pork being analyzed.

Table 4.5 The averaged alpha-diversity indexes calculated for the bacterial communities of *musculus semimembranosus* (SM) samples for high-throughput sequences reads determined at a 97% similarity.

Attribute	Storage time (days)			
	1	4	8	14
Coverage	0.9961 ± 0.0037	0.9972 ± 0.0019	0.9946 ± 0.0033	0.9922 ± 0.0071
Chao 1	686.22 ± 599.15	494.77 ± 281.57	1018.84 ± 579.33	1386.43 ± 1223.79
ACE	746.83 ± 646.73	559.08 ± 315.78	1122.67 ± 651.89	1500.48 ± 1344.33
Shannon	2.16 ± 0.27^{a}	1.06 ± 0.1^{c}	1.33 ± 0.14^{bc}	1.67 ± 0.54^{b}
Simpson	0.82 ± 0.02^{a}	0.55 ± 0.03^{c}	0.62 ± 0.05^{bc}	0.66 ± 0.07^{b}

The data with various upper lowercase letters in each vertical column indicate the significant difference ($P < 0.05$).

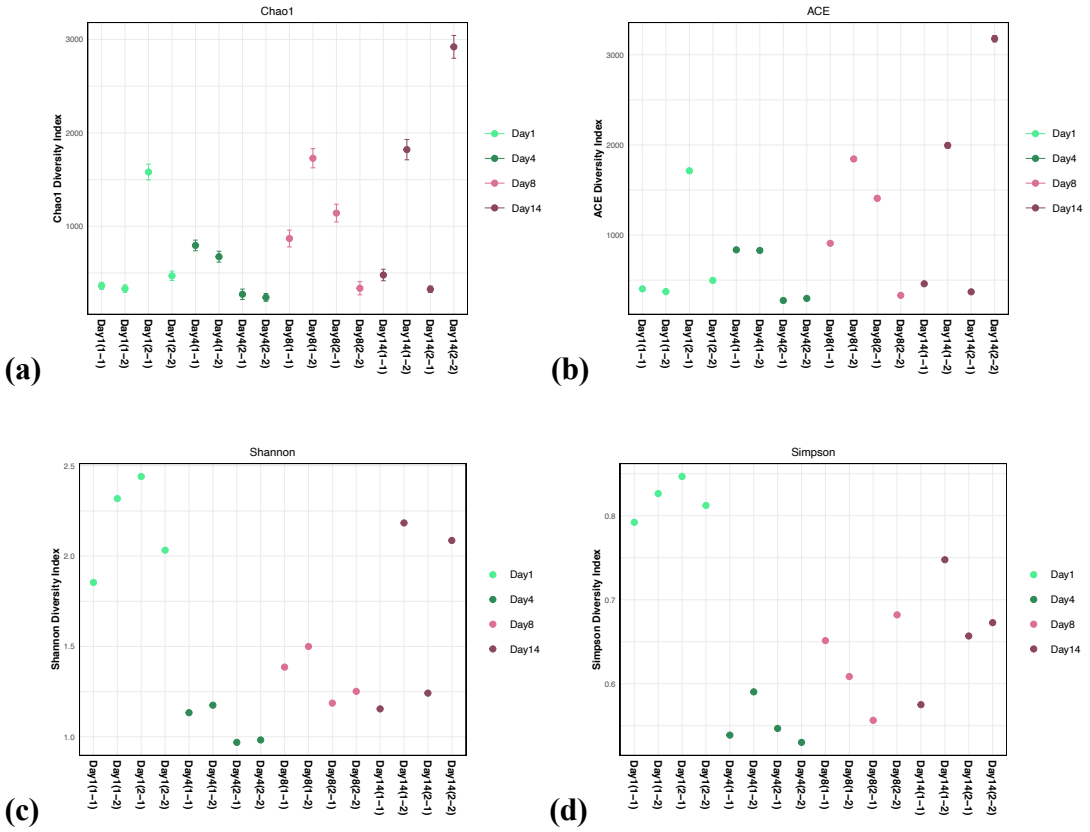

Figure 4.8 Alpha-diversity indexes calculated for the bacterial communities of pork *musculus semimembranosus* (SM) samples for high-throughput sequences reads determined at a 97% similarity. **(a)** Chao1 index. **(b)** ACE index. **(c)** Shannon index. **(d)** Simpson index.

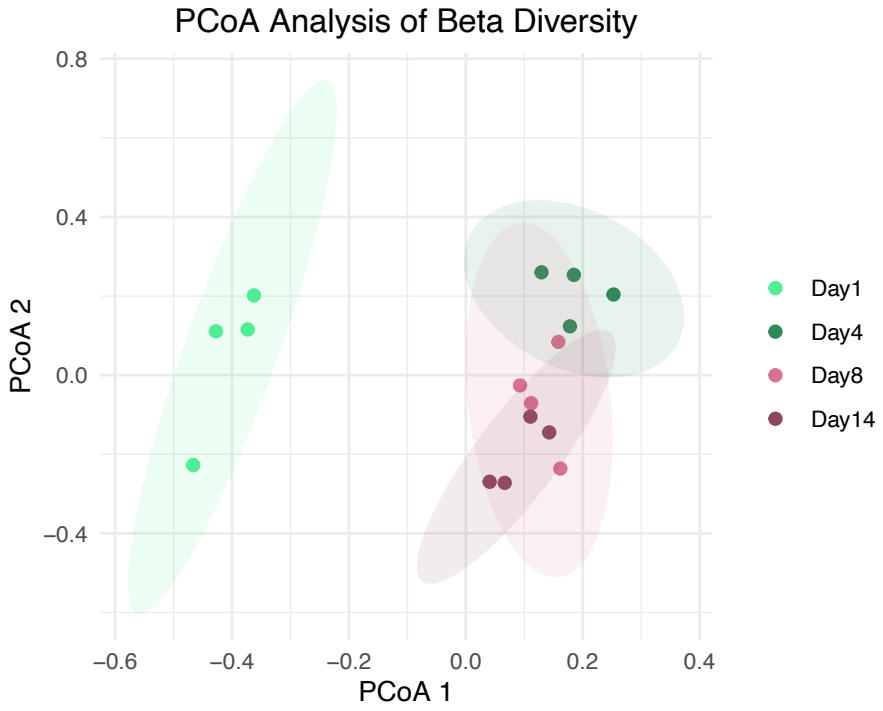

Figure 4.9 Principal co-ordinate analysis (PCoA) of bacterial communities of pork *musculus semimembranosus* (SM) samples.

4.4.2 Composition of bacterial community

4.4.2.1 Pork tenderloin (TL)

The analysis of bacterial community dynamics in pork tenderloin (TL) revealed shifts at both the phylum and genus levels based on relative abundances. At the phylum level, the relative abundance of top 9 phyla during storage were identified and shown in **Figure 4.10** (a), including *Proteobacteria*, *Firmicutes*, *Actinobacteria*, *Bacteroidetes*, *Acidobacteria*, *Chloroflexi*, *Planctomycetes*, *Verrucomicrobia*, and *Fusobacteria*, in a descending order. Specifically, *Proteobacteria* and *Firmicutes* are the major phyla during the whole storage, accounting for ~90%

of all OTUs. Similar observations of predominant phyla were reported in other relevant studies to evaluate bacterial spoilage profiles of pork under refrigerated storage (Wang et al. 2021c; Zhao et al. 2022b). Moreover, as the storage time extended, the percentage of *Proteobacteria* increased and the proportion of *Firmicutes* decreased slightly. **Figure 4.10** (b) displays the changes of relative abundance at the genus level with the top 10 ranking genera characterized. On day 1, *Pseudomonas*, *Stenotrophomonas* and *Acinetobacter* were the dominant genus with close relative abundance within four samples at day 1. As storage progressed, *Pseudomonas* became increasingly dominant from day 4 onwards, while *Stenotrophomonas* and *Acinetobacter* levels significantly reduced, dwindling almost completely by the end of the observation period. These findings align with other studies where *Pseudomonas* was found to be a key contributor to spoilage in chilled pork, often alongside *Acinetobacter* and *Brochothrix* (Peruzy et al. 2019; Wang et al. 2021c; Zhao et al. 2022b). Furthermore, although *Stenotrophomonas* is not typically associated with pork spoilage, it has been identified in other livestock products and quick-frozen foods, indicating its relevance in food spoilage contexts (Zhang et al. 2019).

Pseudomonas is acknowledged as a principal spoilage agent in raw meats, demonstrating a widespread presence across various foodstuffs including fresh pork, beef, poultry, vegetables, milk, and seafood (Raposo et al. 2016). Notably adaptable, Pseudomonas has been detected under numerous environmental conditions, such as ambient air and modified atmosphere packaging (Parlapani et al. 2015). In this study, *Pseudomonas* started with an approximate 25% presence, escalating to around 75% by the end of the storage period, a pattern that echoes findings from previous research (Li et al. 2019). Both *Pseudomonas* and *Acinetobacter* are known to emit volatile metabolites, typically as byproducts of protein and amino acid catabolism, contributing notably to the generation of total volatile basic nitrogen (TVB-N) (Wang et al. 2018a). Given that TVB-N is commonly used as an indicator of protein spoilage, the increased prevalence of these

bacteria correlates with the observed reduction in protein-associated peaks in Raman spectral analysis (Bekhit et al. 2021).

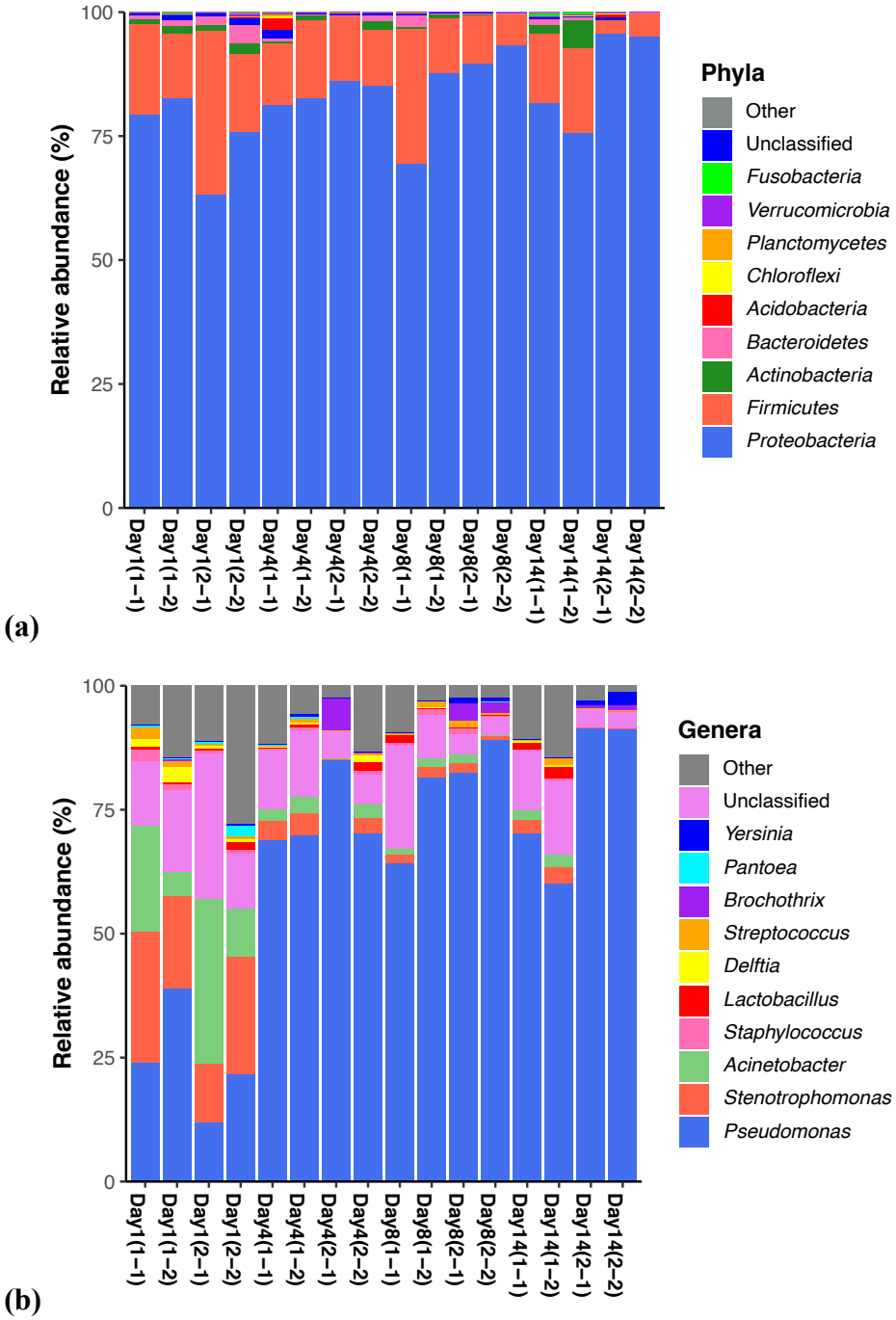

Figure 4.10 Dynamics of relative abundance (%) of bacterial taxa based on 16s rRNA sequencing at phylum **(a)** and genus **(b)** level in pork tenderloin (TL) samples during 14-days storage.

4.4.2.2 Pork musculus semimembranosus (SM)

The bacterial community dynamics of pork SM were also expressed in the form of relative abundance at phylum and genus level and demonstrated in **Figure 4.11**. At the phylum level, top 9 phyla including *Proteobacteria*, *Firmicutes*, *Actinobacteria*, *Bacteroidetes*, *Acidobacteria*, *Gemmatimonadetes*, *Planctomycetes*, *Verrucomicrobia*, and *Thermotogae* are characterized in a descending order. Despite some differences from pork tenderloin (TL) samples, the primary phyla remained consistent, with *Proteobacteria* and *Firmicutes* dominating, together constituting over 95% of all OTUs. The changes of the increasing proportion in *Proteobacteria* as well as decreasing share in *Firmicutes* were also observed. At the genus level, different from genera recognized in pork TL, the top 3 dominant genera in pork SM were *Acinetobacter*, *Pseudomonas*, and *Brochothrix*, which are the most frequently identified genera in pork spoilage process as previously discussed. On day 1, the relative abundance of *Acinetobacter*, *Pseudomonas*, *Brochothrix*, and *Leuconostoc* were close, while *Acinetobacter* and *Brochothrix* were found to be more abundant on day 4. However, by days 8 and 14, *Brochothrix*'s presence diminished, leaving *Acinetobacter* and *Pseudomonas* as the dominant genera. The growth of these spoilage-associated bacteria contributes to the acceleration of spoilage, marked by muscular degradation, discoloration, and off odors (Wang et al. 2021c). Although the relative abundance of dominant bacteria varied irregularly, it was consistent with the changes of the characteristic peaks identified with Raman spectroscopy. The differences between bacterial composition of pork TL and pork SM could be explained by different parts of pork, source of meat, environment and detection time.

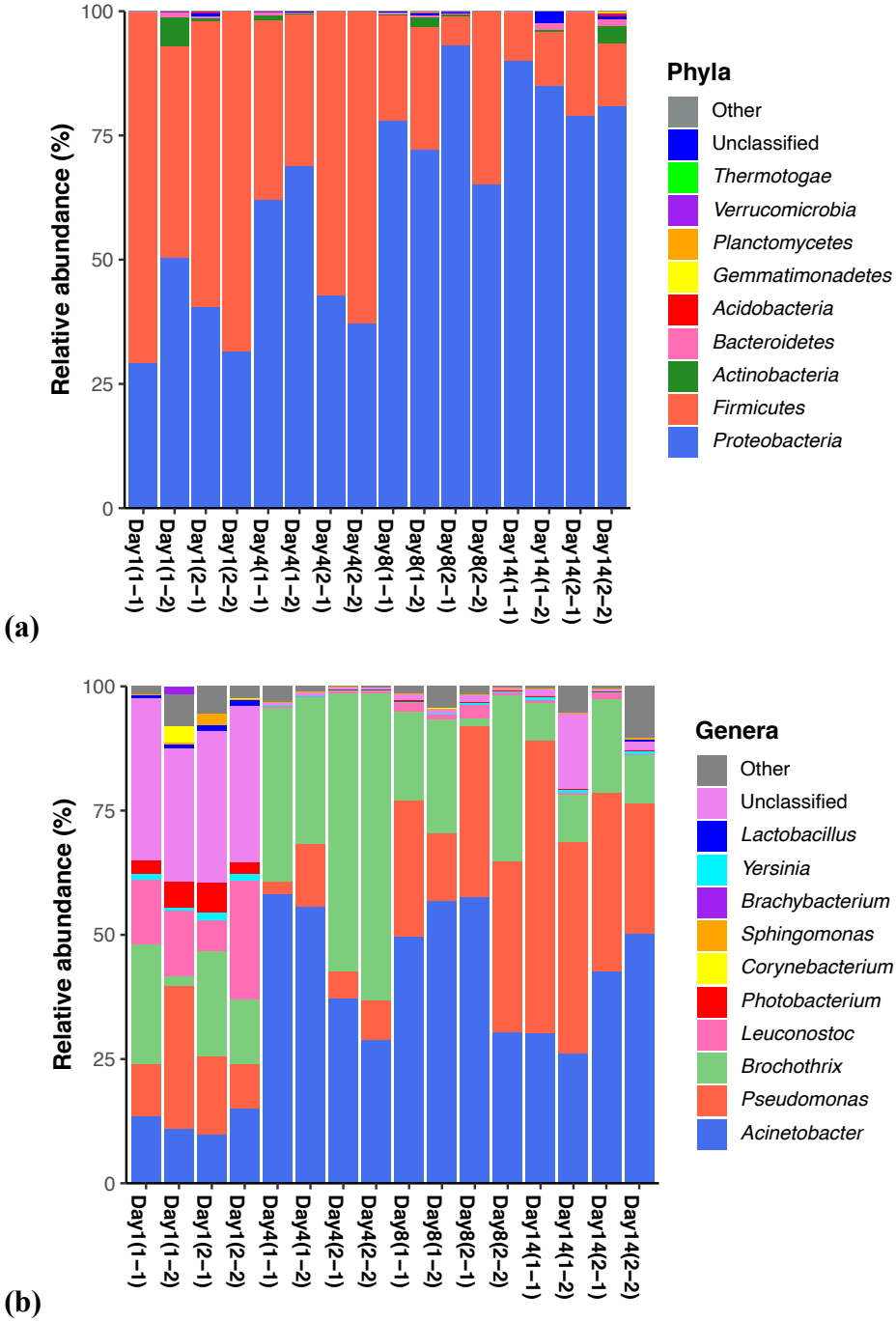

Figure 4.11 Dynamics of relative abundance (%) of bacterial taxa based on 16s rRNA sequencing at phylum **(a)** and genus **(b)** level in pork *musculus semimembranosus* (SM) samples during 14-days storage.

CHAPTER 5. CONCLUSTION

In this study, the capability of Raman spectroscopy combined with chemometrics for rapid *in situ* identification of pork meat spoilage was assessed using pork tenderloin and pork *musculus semimembranosus* samples. To correlate the changes of Raman spectra and bacterial compositions, the bacterial community dynamics of pork tenderloin and pork *musculus semimembranosus* samples during storage at 4°C for 14 days were evaluated using 16S rRNA high-throughput sequencing. Firstly, microbial test of total viable counts was calculated, which revealed that day 4 was the threshold of timepoint to differentiate fresh and spoiled pork samples. In the meantime, Raman spectra were collected with an integration time of 40 s and laser power of 250 mW. Furthermore, chemometrics including PCA and several supervised machine learning algorithms were applied to solve 2-group classification problem. Although the separation in PCA was not obvious, CNNs deep learning algorithm could provide > 90% accuracy to identify and differentiate fresh and spoiled pork samples. In addition, Next-generation sequencing data pinpointed *Proteobacteria* and *Firmicutes* as the dominant phyla in both pork tenderloin and pork musculus *semimembranosus*, while at the genus level, *Pseudomonas*, *Stenotrophomonas*, and *Acinetobacter* were prevalent in pork tenderloin, and *Acinetobacter*, *Pseudomonas*, and *Brochothrix* in pork musculus *semimembranosus*. Notably, the shift in bacterial communities during spoilage paralleled changes in the characteristic Raman spectral peaks, underscoring the synergy between microbial shifts and spectroscopic signatures.

To the best of our knowledge, this study represents a pioneering effort to integrate portable Raman spectroscopy with machine learning algorithms and high-throughput sequencing for the identification of pork spoilage. Our findings confirm that Raman spectroscopy is a powerful tool, capable of rapidly and non-destructively distinguishing between fresh and spoiled pork with high

precision. The development of an extensive Raman spectral database, enriched by future studies incorporating a larger number of replicates, will further solidify the potential of this technique. It holds great promise for becoming a standard, quick-screening method that could be deployed throughout the pork supply chain for ensuring meat quality and safety.

REFERENCES

Alexander, R., Uppal, S., Dey, A., Kaushal, A., Prakash, J., & Dasgupta, K. (2023). Machine learning approach for label-free rapid detection and identification of virus using Raman spectra. *Intelligent Medicine*, *3*, 22–35.

Angel, S. M., Carrabba, M., & Cooney, T. F. (1995). The utilization of diode lasers for Raman spectroscopy. *Spectrochimica Acta Part A: Molecular and Biomolecular Spectroscopy*, *51*, 1779–1799.

Argyri, A. A., Jarvis, R. M., Wedge, D., Xu, Y., Panagou, E. Z., Goodacre, R., & Nychas, G.-J. E. (2013). A comparison of Raman and FT-IR spectroscopy for the prediction of meat spoilage. *Food Control*, *29*, 461–470.

Balage, J. M., da Luz e Silva, S., Gomide, C. A., Bonin, M. de N., & Figueira, A. C. (2015). Predicting pork quality using Vis/NIR spectroscopy. *Meat Science*, *108*, 37–43.

Barbin, D. F., ElMasry, G., Sun, D.-W., Allen, P., & Morsy, N. (2013). Non-destructive assessment of microbial contamination in porcine meat using NIR hyperspectral imaging. *Innovative Food Science & Emerging Technologies*, *17*, 180–191.

Bekhit, A. E.-D. A., Holman, B. W. B., Giteru, S. G., & Hopkins, D. L. (2021). Total volatile basic nitrogen (TVB-N) and its role in meat spoilage: A review. *Trends in Food Science & Technology*, *109*, 280–302.

Bocklitz, T., Walter, A., Hartmann, K., Rösch, P., & Popp, J. (2011). How to pre-process Raman spectra for reliable and stable models? *Analytica Chimica Acta*, *704*, 47–56.

Bowker, B., & Zhuang, H. (2015). Relationship between water-holding capacity and protein denaturation in broiler breast meat. *Poultry Science*, *94*, 1657–1664.

Brereton, R. G. (2007). *Applied Chemometrics for Scientists*. John Wiley & Sons.

Brown, S., Tauler, R., & Walczak, B. (2020). *Comprehensive Chemometrics: Chemical and Biochemical Data Analysis*. Elsevier.

Bukin, Y. S., Galachyants, Y. P., Morozov, I. V., Bukin, S. V., Zakharenko, A. S., & Zemskaya, T. I. (2019). The effect of 16S rRNA region choice on bacterial community metabarcoding results. *Scientific Data*, *6*, 190007.

Butler, H. J., Ashton, L., Bird, B., Cinque, G., Curtis, K., Dorney, J., … Martin, F. L. (2016). Using Raman spectroscopy to characterize biological materials. *Nature Protocols*, *11*, 664–687.

Byrne, H. J., Knief, P., Keating, M. E., & Bonnier, F. (2016). Spectral pre and post processing for infrared and Raman spectroscopy of biological tissues and cells. *Chemical Society Reviews*, *45*, 1865–1878.

Cai, J., Zou, C., Yin, L., Jiang, S., El-Seedi, H. R., & Guo, Z. (2023). Characterization and recognition of citrus fruit spoilage fungi using Raman scattering spectroscopic imaging. *Vibrational Spectroscopy*, *124*, 103474.

Chaillou, S., Chaulot-Talmon, A., Caekebeke, H., Cardinal, M., Christieans, S., Denis, C., … Champomier-Vergès, M.-C. (2015). Origin and ecological selection of core and food-specific bacterial communities associated with meat and seafood spoilage. *The ISME Journal*, *9*, 1105–1118.

Chase, B. (1994). A New Generation of Raman Instrumentation. *Applied Spectroscopy*, *48*, 14A-19A.

Chen, D. (2021). Analysis of Machine Learning Methods for COVID-19 Detection Using Serum Raman Spectroscopy. *Applied Artificial Intelligence*, *35*, 1147–1168.

Chen, J., Gu, J., Zhang, R., Mao, Y., & Tian, S. (2019). Freshness Evaluation of Three Kinds of Meats Based on the Electronic Nose. *Sensors*, *19*, 605.

Cheng, J.-H., & Sun, D.-W. (2015). Recent Applications of Spectroscopic and Hyperspectral Imaging Techniques with Chemometric Analysis for Rapid Inspection of Microbial Spoilage in Muscle Foods. *Comprehensive Reviews in Food Science and Food Safety*, *14*, 478–490.

Cheng, L., Sun, D.-W., Zhu, Z., & Zhang, Z. (2017). Emerging techniques for assisting and accelerating food freezing processes: A review of recent research progresses. *Critical Reviews in Food Science and Nutrition*, *57*, 769–781.

Chi, Z., Chen, X. G., Holtz, J. S. W., & Asher, S. A. (1998). UV Resonance Raman-Selective Amide Vibrational Enhancement: Quantitative Methodology for Determining Protein Secondary Structure. *Biochemistry*, *37*, 2854–2864.

Chicco, D., & Jurman, G. (2020). The advantages of the Matthews correlation coefficient (MCC) over F1 score and accuracy in binary classification evaluation. *BMC Genomics*, *21*, 6.

Coombs, C. E. O., Holman, B. W. B., Friend, M. A., & Hopkins, D. L. (2017). Long-term red meat preservation using chilled and frozen storage combinations: A review. *Meat Science*, *125*, 84–94.

Czamara, K., Majzner, K., Pacia, M. Z., Kochan, K., Kaczor, A., & Baranska, M. (2015). Raman spectroscopy of lipids: A review. *Journal of Raman Spectroscopy*, *46*, 4–20.

Das, R. S., & Agrawal, Y. K. (2011). Raman spectroscopy: Recent advancements, techniques and applications. *Vibrational Spectroscopy*, *57*, 163–176.

De Gelder, J., De Gussem, K., Vandenabeele, P., & Moens, L. (2007). Reference database of Raman spectra of biological molecules. *Journal of Raman Spectroscopy*, *38*, 1133–1147.

Díaz, P., Nieto, G., Garrido, M. D., & Bañón, S. (2008). Microbial, physical–chemical and sensory spoilage during the refrigerated storage of cooked pork loin processed by the sous vide method. *Meat Science*, *80*, 287–292.

Dissing, B. S., Papadopoulou, O. S., Tassou, C., Ersbøll, B. K., Carstensen, J. M., Panagou, E. Z., & Nychas, G.-J. (2013). Using Multispectral Imaging for Spoilage Detection of Pork Meat. *Food and Bioprocess Technology*, *6*, 2268–2279.

Doulgeraki, A. I., Ercolini, D., Villani, F., & Nychas, G.-J. E. (2012). Spoilage microbiota associated to the storage of raw meat in different conditions. *International Journal of Food Microbiology*, *157*, 130–141.

Dreiseitl, S., & Ohno-Machado, L. (2002). Logistic regression and artificial neural network classification models: A methodology review. *Journal of Biomedical Informatics*, *35*, 352–359.

Du, Y., Han, D., Liu, S., Sun, X., Ning, B., Han, T., … Gao, Z. (2022). Raman spectroscopy-based adversarial network combined with SVM for detection of foodborne pathogenic bacteria. *Talanta*, *237*, 122901.

Duun, A. S., & Rustad, T. (2007). Quality changes during superchilled storage of cod (Gadus morhua) fillets. *Food Chemistry*, *105*, 1067–1075.

Elmasry, G., Barbin, D. F., Sun, D.-W., & Allen, P. (2012). Meat Quality Evaluation by Hyperspectral Imaging Technique: An Overview. *Critical Reviews in Food Science and Nutrition*, *52*, 689–711.

E. Masson, L., M. O'Brien, C., J. Pence, I., L. Herington, J., Reese, J., Leeuwen, T. G. van, & Mahadevan-Jansen, A. (2018). Dual excitation wavelength system for combined fingerprint and high wavenumber Raman spectroscopy. *Analyst*, *143*, 6049–6060.

Enfors, S.-O., Molin, G., & Ternström, A. (1979). Effect of Packaging under Carbon Dioxide, Nitrogen or Air on the Microbial Flora of Pork Stored at 4°C. *Journal of Applied Bacteriology*, *47*, 197–208.

Feifei, T., Yankun, P., & Yongyu, L. (2015). Feature extraction method of hyperspectral scattering images for prediction of total viable count in pork meat. *International Journal of Agricultural and Biological Engineering*, *8*, 95–105.

Fengou, L.-C., Spyrelli, E., Lianou, A., Tsakanikas, P., Panagou, E. Z., & Nychas, G.-J. E. (2019). Estimation of Minced Pork Microbiological Spoilage through Fourier Transform Infrared and Visible Spectroscopy and Multispectral Vision Technology. *Foods*, *8*, 238.

Fuentes, A. M., Narayan, A., Milligan, K., Lum, J. J., Brolo, A. G., Andrews, J. L., & Jirasek, A. (2023). Raman spectroscopy and convolutional neural networks for monitoring biochemical radiation response in breast tumour xenografts. *Scientific Reports*, *13*, 1530.

Fukuhara, M., Fujiwara, K., Maruyama, Y., & Itoh, H. (2019). Feature visualization of Raman spectrum analysis with deep convolutional neural network. *Analytica Chimica Acta*, *1087*, 11–19.

Gautam, R., Vanga, S., Ariese, F., & Umapathy, S. (2015). Review of multidimensional data processing approaches for Raman and infrared spectroscopy. *EPJ Techniques and Instrumentation*, *2*, 1–38.

Gil, L., Barat, J. M., Baigts, D., Martínez-Máñez, R., Soto, J., Garcia-Breijo, E., … Llobet, E. (2011). Monitoring of physical–chemical and microbiological changes in fresh pork meat under cold storage by means of a potentiometric electronic tongue. *Food Chemistry*, *126*, 1261–1268.

Gill, C. O. (1983). Meat Spoilage and Evaluation of the Potential Storage Life of Fresh Meat. *Journal of Food Protection*, *46*, 444–452.

Girolami, A., Napolitano, F., Faraone, D., & Braghieri, A. (2013). Measurement of meat color using a computer vision system. *Meat Science*, *93*, 111–118.

Godziszewska, J., Guzek, D., Pogorzelska, E., Brodowska, M., Górska-Horczyczak, E., Sakowska, A., … Wierzbicka, A. (2017). A simple method of the detection of pork spoilage caused by Rahnella aquatilis. *LWT*, *84*, 248–255.

Gu, H., Wang, Y., Hong, S., & Gui, G. (2019). Blind Channel Identification Aided Generalized Automatic Modulation Recognition Based on Deep Learning. *IEEE Access*, *PP*, 1–1.

Gu, X., Feng, L., Zhu, J., Li, Y., Tu, K., Dong, Q., & Pan, L. (2021). Application of gas sensors for modelling the dynamic growth of Pseudomonas in pork stored at different temperatures. *Meat Science*, *171*, 108282.

Guo, S., Popp, J., & Bocklitz, T. (2021). Chemometric analysis in Raman spectroscopy from experimental design to machine learning–based modeling. *Nature Protocols*, *16*, 5426–5459.

Guo, Z., Wang, M., Barimah, A. O., Chen, Q., Li, H., Shi, J., … Zou, X. (2021). Label-free surface enhanced Raman scattering spectroscopy for discrimination and detection of dominant apple spoilage fungus. *International Journal of Food Microbiology*, *338*, 108990.

Haka, A. S., Volynskaya, Z. I., Gardecki, J. A., Nazemi, J., Shenk, R., Wang, N., … Feld, M. S. (2009). Diagnosing breast cancer using Raman spectroscopy: Prospective analysis. *Journal of Biomedical Optics*, *14*, 054023.

He, S., Zhang, W., Liu, L., Huang, Y., He, J., Xie, W., … Du, C. (2014). Baseline correction for Raman spectra using an improved asymmetric least squares method. *Anal. Methods*, *6*, 4402–4407.

Heino, J., Melo, A. S., & Bini, L. M. (2015). Reconceptualising the beta diversity-environmental heterogeneity relationship in running water systems. *Freshwater Biology*, *60*, 223–235.

Ho, C.-S., Jean, N., Hogan, C. A., Blackmon, L., Jeffrey, S. S., Holodniy, M., … Dionne, J. (2019). Rapid identification of pathogenic bacteria using Raman spectroscopy and deep learning. *Nature Communications*, *10*, 4927.

Holman, B. W. B., Mao, Y., Coombs, C. E. O., van de Ven, R. J., & Hopkins, D. L. (2016). Relationship between colorimetric (instrumental) evaluation and consumer-defined beef colour acceptability. *Meat Science*, *121*, 104–106.

Horváth, K., Seregély, Z., Andrássy, É., Dalmadi, I., & Farkas, J. (2008). A preliminary study using near infrared spectroscopy to evaluate freshness and detect spoilage in sliced pork meat. *Acta Alimentaria*, *37*, 93–102.

Hu, R., Zhang, M., & Mujumdar, A. S. (2022). Application of infrared and microwave heating prior to freezing of pork: Effect on frozen meat quality. *Meat Science*, *189*, 108811.

Huang, L., Zhao, J., Chen, Q., & Zhang, Y. (2013). Rapid detection of total viable count (TVC) in pork meat by hyperspectral imaging. *Food Research International*, *54*, 821–828.

Huang, L., Zhao, J., Chen, Q., & Zhang, Y. (2014). Nondestructive measurement of total volatile basic nitrogen (TVB-N) in pork meat by integrating near infrared spectroscopy, computer vision and electronic nose techniques. *Food Chemistry*, *145*, 228–236.

Huff-Lonergan, E., & Lonergan, S. M. (2005). Mechanisms of water-holding capacity of meat: The role of postmortem biochemical and structural changes. *Meat Science*, *71*, 194–204.

Ilie, A. G., Scarisoareanu, M., Morjan, I., Dutu, E., Badiceanu, M., & Mihailescu, I. (2017). Principal component analysis of Raman spectra for TiO2 nanoparticle characterization. *Applied Surface Science*, *417*, 93–103.

Jaafreh, S., Breuch, R., Günther, K., Kreyenschmidt, J., & Kaul, P. (2018). Rapid Poultry Spoilage Evaluation Using Portable Fiber-Optic Raman Spectrometer. *Food Analytical Methods*, *11*, 2320–2328.

Jaafreh, S., Valler, O., Kreyenschmidt, J., Günther, K., & Kaul, P. (2019). In vitro discrimination and classification of Microbial Flora of Poultry using two dispersive Raman spectrometers (microscope and Portable Fiber-Optic systems) in tandem with chemometric analysis. *Talanta*, *202*, 411–425.

Janda, J. M., & Abbott, S. L. (2007). 16S rRNA Gene Sequencing for Bacterial Identification in the Diagnostic Laboratory: Pluses, Perils, and Pitfalls. *Journal of Clinical Microbiology*, *45*, 2761–2764.

Jin, H., Lu, Q., Chen, X., Ding, H., Gao, H., & Jin, S. (2016). The use of Raman spectroscopy in food processes: A review. *Applied Spectroscopy Reviews*, *51*, 12–22.

Johnson, J. S., Spakowicz, D. J., Hong, B.-Y., Petersen, L. M., Demkowicz, P., Chen, L., … Weinstock, G. M. (2019). Evaluation of 16S rRNA gene sequencing for species and strain-level microbiome analysis. *Nature Communications*, *10*, 5029.

Kaale, L. D., Eikevik, T. M., Rustad, T., & Kolsaker, K. (2011). Superchilling of food: A review. *Journal of Food Engineering*, *107*, 141–146.

Kamruzzaman, M., Makino, Y., & Oshita, S. (2015). Non-invasive analytical technology for the detection of contamination, adulteration, and authenticity of meat, poultry, and fish: A review. *Analytica Chimica Acta*, *853*, 19–29.

Kapper, C., Walukonis, C. J., Scheffler, T. L., Scheffler, J. M., Don, C., Morgan, M. T., … Gerrard, D. E. (2014). Moisture absorption early postmortem predicts ultimate drip loss in fresh pork. *Meat Science*, *96*, 971–976.

Kazemzadeh, M., Hisey, C. L., Zargar-Shoshtari, K., Xu, W., & Broderick, N. G. R. (2022). Deep convolutional neural networks as a unified solution for Raman spectroscopy-based classification in biomedical applications. *Optics Communications*, *510*, 127977.

Kelis Cardoso, V. G., & Poppi, R. J. (2021). Cleaner and faster method to detect adulteration in cassava starch using Raman spectroscopy and one-class support vector machine. *Food Control*, *125*, 107917.

Kemp, P. F., & Aller, J. Y. (2004). Bacterial diversity in aquatic and other environments: What 16S rDNA libraries can tell us. *FEMS Microbiology Ecology*, *47*, 161–177.

Khaled, A. Y., Parrish, C. A., & Adedeji, A. (2021). Emerging nondestructive approaches for meat quality and safety evaluation—A review. *Comprehensive Reviews in Food Science and Food Safety*, *20*, 3438–3463.

Kim, H., Trinh, B. T., Kim, K. H., Moon, J., Kang, H., Jo, K., … Kang, T. (2021). Au@ZIF-8 SERS paper for food spoilage detection. *Biosensors and Bioelectronics*, *179*, 113063.

Kim, H.-J., & Jang, A. (2018). Evaluation of the microbiological status of raw pork meat in Korea: Modification of the microbial guideline levels for meat. *Food Science and Biotechnology*, *27*, 1219–1225.

Koomkrong, N., Gongruttananun, N., Boonkaewwan, C., Noosud, J., Theerawatanasirikul, S., & Kayan, A. (2017). Fiber characteristics of pork muscle exhibiting different levels of drip loss. *Animal Science Journal*, *88*, 2044–2049.

Kozich, J. J., Westcott, S. L., Baxter, N. T., Highlander, S. K., & Schloss, P. D. (2013). Development of a Dual-Index Sequencing Strategy and Curation Pipeline for Analyzing Amplicon Sequence Data on the MiSeq Illumina Sequencing Platform. *Applied and Environmental Microbiology*, *79*, 5112–5120.

Kucha, C. T., & Ngadi, M. O. (2020). Rapid assessment of pork freshness using miniaturized NIR spectroscopy. *Journal of Food Measurement and Characterization*, *14*, 1105–1115.

Kühn, S., Düzel, S., Colzato, L., Norman, K., Gallinat, J., Brandmaier, A. M., … Widaman, K. F. (2019). Food for thought: Association between dietary tyrosine and cognitive performance in younger and older adults. *Psychological Research*, *83*, 1097–1106.

Leng, T., Li, F., Chen, Y., Tang, L., Xie, J., & Yu, Q. (2021). Fast quantification of total volatile basic nitrogen (TVB-N) content in beef and pork by near-infrared spectroscopy: Comparison of SVR and PLS model. *Meat Science*, *180*, 108559.

Leygonie, C., Britz, T. J., & Hoffman, L. C. (2012). Impact of freezing and thawing on the quality of meat: Review. *Meat Science*, *91*, 93–98.

Li, Hongtao, Wang, S., Zeng, Q., Chen, C., Lv, X., Ma, M., … Fang, J. (2022). Serum Raman spectroscopy combined with multiple classification models for rapid diagnosis of breast cancer. *Photodiagnosis and Photodynamic Therapy*, *40*, 103115.

Li, Huanhuan, Geng, W., Haruna, S. A., Zhou, C., Wang, Y., Ouyang, Q., & Chen, Q. (2022). Identification of characteristic volatiles and metabolomic pathway during pork storage using HS-SPME-GC/MS coupled with multivariate analysis. *Food Chemistry*, *373*, 131431.

Li, Huanhuan, Sun, X., Pan, W., Kutsanedzie, F., Zhao, J., & Chen, Q. (2016). Feasibility study on nondestructively sensing meat's freshness using light scattering imaging technique. *Meat Science*, *119*, 102–109.

Li, M., Wang, H., Sun, L., Zhao, G., & Huang, X. (2016). Application of Electronic Nose for Measuring Total Volatile Basic Nitrogen and Total Viable Counts in Packaged Pork During Refrigerated Storage. *Journal of Food Science*, *81*, M906–M912.

Li, N., Zhang, Y., Wu, Q., Gu, Q., Chen, M., Zhang, Y., … Zhang, J. (2019). High-throughput sequencing analysis of bacterial community composition and quality characteristics in refrigerated pork during storage. *Food Microbiology*, *83*, 86–94.

Li, Y.-S., & Church, J. S. (2014). Raman spectroscopy in the analysis of food and pharmaceutical nanomaterials. *Journal of Food and Drug Analysis*, *22*, 29–48.

Lieber, C. A., & Mahadevan-Jansen, A. (2003). Automated Method for Subtraction of Fluorescence from Biological Raman Spectra. *Applied Spectroscopy*, *57*, 1363–1367.

Lieber, C. A., Majumder, S. K., Billheimer, D. D., M.d, D. L. E., & Mahadevan-Jansen, A. (2009). Raman microspectroscopy for skin cancer detection in vitro. *Journal of Biomedical Optics*, *13*, 024013.

Limbo, S., Sinelli, N., Torri, L., & Riva, M. (2009). Freshness decay and shelf-life predictive modelling of European sea bass (Dicentrarchus labrax) applying chemical methods and electronic nose. *LWT - Food Science and Technology*, *42*, 977–984.

Liu, H., Saito, Y., Riza, D. F. A., Kondo, N., Yang, X., & Han, D. (2019). Rapid evaluation of quality deterioration and freshness of beef during low temperature storage using three-dimensional fluorescence spectroscopy. *Food Chemistry*, *287*, 369–374.

Liu, J., Osadchy, M., Ashton, L., Foster, M., J. Solomon, C., & J. Gibson, S. (2017). Deep convolutional neural networks for Raman spectrum recognition: A unified solution. *Analyst*, *142*, 4067–4074.

Liu, Q., Dong, P., Fengou, L.-C., Nychas, G.-J., Fowler, S. M., Mao, Y., … Zhang, Y. (2023). Preliminary investigation into the prediction of indicators of beef spoilage using Raman and Fourier transform infrared spectroscopy. *Meat Science*, *200*, 109168.

Lu, X., Zhang, Y., Zhu, L., Luo, X., & Hopkins, D. L. (2019). Effect of superchilled storage on shelf life and quality characteristics of M. longissimus lumborum from Chinese Yellow cattle. *Meat Science*, *149*, 79–84.

Lussier, F., Thibault, V., Charron, B., Wallace, G. Q., & Masson, J.-F. (2020). Deep learning and artificial intelligence methods for Raman and surface-enhanced Raman scattering. *TrAC Trends in Analytical Chemistry*, *124*, 115796.

Ma, D., Shang, L., Tang, J., Bao, Y., Fu, J., & Yin, J. (2021). Classifying breast cancer tissue by Raman spectroscopy with one-dimensional convolutional neural network. *Spectrochimica Acta Part A: Molecular and Biomolecular Spectroscopy*, *256*, 119732.

McMillin, K. W. (2008). Where is MAP Going? A review and future potential of modified atmosphere packaging for meat. *Meat Science*, *80*, 43–65.

McMillin, K. W. (2017). Advancements in meat packaging. *Meat Science*, *132*, 153–162.

Modi, A., Vai, S., Caramelli, D., & Lari, M. (2021). The Illumina Sequencing Protocol and the NovaSeq 6000 System. In A. Mengoni, G. Bacci, & M. Fondi (Eds.), *Bacterial Pangenomics: Methods and Protocols* (pp. 15–42). New York, NY: Springer US.

Motoyama, M., Kobayashi, M., Sasaki, K., Nomura, M., & Mitsumoto, M. (2010). Pseudomonas spp. Convert metmyoglobin into deoxymyoglobin. *Meat Science*, *84*, 202–207.

Movasaghi, Z., Rehman, S., & Rehman, I. U. (2007). Raman Spectroscopy of Biological Tissues. *Applied Spectroscopy Reviews*, *42*, 493–541.

Muela, E., Sañudo, C., Campo, M. M., Medel, I., & Beltrán, J. A. (2010). Effect of freezing method and frozen storage duration on instrumental quality of lamb throughout display. *Meat Science*, *84*, 662–669.

Müller, A., Marschall, S., Jensen, O. B., Fricke, J., Wenzel, H., Sumpf, B., & Andersen, P. E. (2013). Diode laser based light sources for biomedical applications. *Laser & Photonics Reviews*, *7*, 605–627.

Munekata, P. E. S., Finardi, S., de Souza, C. K., Meinert, C., Pateiro, M., Hoffmann, T. G., … Lorenzo, J. M. (2023). Applications of Electronic Nose, Electronic Eye and Electronic

Tongue in Quality, Safety and Shelf Life of Meat and Meat Products: A Review. *Sensors*, *23*, 672.

Narasimha Rao, D., & Sachindra, N. M. (2002). Modified Atmosphere and Vacuum Packaging of Meat and Poultry Products. *Food Reviews International*, *18*, 263–293.

Nawrocka, A., Szymańska-Chargot, M., Miś, A., Wilczewska, A. Z., & Markiewicz, K. H. (2016). Dietary Fiber-Induced Changes in the Structure and Thermal Properties of Gluten Proteins Studied by Fourier Transform-Raman Spectroscopy and Thermogravimetry. *Journal of Agricultural and Food Chemistry*, *64*, 2094–2104.

Norman, J. L., Berg, E. P., Ellersieck, M. R., & Lorenzen, C. L. (2004). Prediction of color and pH measurement throughout boneless center-cut pork loins. *Meat Science*, *66*, 273–278.

Nychas, G.-J. E., Skandamis, P. N., Tassou, C. C., & Koutsoumanis, K. P. (2008). Meat spoilage during distribution. *Meat Science*, *78*, 77–89.

O'Brien, C. M., Herington, J. L., Brown, N., Pence, I. J., Paria, B. C., Slaughter, J. C., … Mahadevan-Jansen, A. (2017). In vivo Raman spectral analysis of impaired cervical remodeling in a mouse model of delayed parturition. *Scientific Reports*, *7*, 6835.

Orlando, A., Franceschini, F., Muscas, C., Pidkova, S., Bartoli, M., Rovere, M., & Tagliaferro, A. (2021). A Comprehensive Review on Raman Spectroscopy Applications. *Chemosensors*, *9*, 262.

Özbalci, B., Boyaci, İ. H., Topcu, A., Kadılar, C., & Tamer, U. (2013). Rapid analysis of sugars in honey by processing Raman spectrum using chemometric methods and artificial neural networks. *Food Chemistry*, *136*, 1444–1452.

Pan, L., Zhang, P., Daengngam, C., Peng, S., & Chongcheawchamnan, M. (2022). A review of artificial intelligence methods combined with Raman spectroscopy to identify the composition of substances. *Journal of Raman Spectroscopy*, *53*, 6–19.

Papadopoulou, O., Panagou, E. Z., Tassou, C. C., & Nychas, G.-J. E. (2011). Contribution of Fourier transform infrared (FTIR) spectroscopy data on the quantitative determination of minced pork meat spoilage. *Food Research International*, *44*, 3264–3271.

Park, S. T., & Kim, J. (2016). Trends in Next-Generation Sequencing and a New Era for Whole Genome Sequencing. *International Neurourology Journal*, *20*, S76-83.

Parlapani, F. F., Kormas, K. A., & Boziaris, I. S. (2015). Microbiological changes, shelf life and identification of initial and spoilage microbiota of sea bream fillets stored under various conditions using 16S rRNA gene analysis. *Journal of the Science of Food and Agriculture*, *95*, 2386–2394.

Patel, H., & Prajapati, P. (2018). Study and Analysis of Decision Tree Based Classification Algorithms. *International Journal of Computer Sciences and Engineering*, *6*, 74–78.

Pellissery, A. J., Vinayamohan, P. G., Amalaradjou, M. A. R., & Venkitanarayanan, K. (2020). Chapter 17—Spoilage bacteria and meat quality. In A. K. Biswas & P. K. Mandal (Eds.), *Meat Quality Analysis* (pp. 307–334). Academic Press.

Penny, K. I., & Jolliffe, I. T. (2001). A Comparison of Multivariate Outlier Detection Methods for Clinical Laboratory Safety Data. *Journal of the Royal Statistical Society: Series D (The Statistician)*, *50*, 295–307.

Peruzy, M. F., Murru, N., Yu, Z., Cnockaert, M., Joossens, M., Proroga, Y. T. R., & Houf, K. (2019). Determination of the microbiological contamination in minced pork by culture dependent and 16S amplicon sequencing analysis. *International Journal of Food Microbiology*, *290*, 27–35.

Pinheiro, R. S. B., Francisco, C. L., Lino, D. M., & Borba, H. (2019). Meat quality of Santa Inês lamb chilled-then-frozen storage up to 12 months. *Meat Science*, *148*, 72–78.

Prabhakar, P. K., Srivastav, P. P., & Pathak, S. S. (2019). Kinetics of Total Volatile Basic Nitrogen and Trimethylamine Formation in Stored Rohu (Labeo rohita) Fish. *Journal of Aquatic Food Product Technology*, *28*, 452–464.

Pu, H., Yu, J., Sun, D.-W., Wei, Q., Shen, X., & Wang, Z. (2023). Distinguishing fresh and frozen-thawed beef using hyperspectral imaging technology combined with convolutional neural networks. *Microchemical Journal*, *189*, 108559.

Qi, Y., Hu, D., Jiang, Y., Wu, Z., Zheng, M., Chen, E. X., … Chen, Y. P. (2023). Recent Progresses in Machine Learning Assisted Raman Spectroscopy. *Advanced Optical Materials*, *11*, 2203104.

Quast, C., Pruesse, E., Yilmaz, P., Gerken, J., Schweer, T., Yarza, P., … Glöckner, F. O. (2013). The SILVA ribosomal RNA gene database project: Improved data processing and web-based tools. *Nucleic Acids Research*, *41*, D590–D596.

Raposo, A., Pérez, E., de Faria, C. T., Ferrús, M. A., & Carrascosa, C. (2016). Food Spoilage by Pseudomonas spp.—An Overview. In *Foodborne Pathogens and Antibiotic Resistance* (pp. 41–71). John Wiley & Sons, Ltd.

Rodriguez, S. B., Thornton, M. A., & Thornton, R. J. (2013). Raman Spectroscopy and Chemometrics for Identification and Strain Discrimination of the Wine Spoilage Yeasts Saccharomyces cerevisiae, Zygosaccharomyces bailii, and Brettanomyces bruxellensis. *Applied and Environmental Microbiology*, *79*, 6264–6270.

Ryabchykov, O., Bocklitz, T., Ramoji, A., Neugebauer, U., Foerster, M., Kroegel, C., … Popp, J. (2016). Automatization of spike correction in Raman spectra of biological samples. *Chemometrics and Intelligent Laboratory Systems*, *155*, 1–6.

Rygula, A., Majzner, K., Marzec, K. M., Kaczor, A., Pilarczyk, M., & Baranska, M. (2013). Raman spectroscopy of proteins: A review. *Journal of Raman Spectroscopy*, *44*, 1061–1076.

Sachdev, D., Kumar, V., Maheshwari, P. H., Pasricha, R., Deepthi, & Baghel, N. (2016). Silver based nanomaterial, as a selective colorimetric sensor for visual detection of post harvest spoilage in onion. *Sensors and Actuators B: Chemical*, *228*, 471–479.

Santos, C. C., Zhao, J., Dong, X., Lonergan, S. M., Huff- Lonergan, E., Outhouse, A., … Wheeler, T. L. (2018). Predicting aged pork quality using a portable Raman device. *Meat Science*, *145*, 79–85.

Savitzky, Abraham., & Golay, M. J. E. (1964). Smoothing and Differentiation of Data by Simplified Least Squares Procedures. *Analytical Chemistry*, *36*, 1627–1639.

Schluenzen, F., Tocilj, A., Zarivach, R., Harms, J., Gluehmann, M., Janell, D., … Yonath, A. (2000). Structure of Functionally Activated Small Ribosomal Subunit at 3.3 Å Resolution. *Cell*, *102*, 615–623.

Schmidt, H., Sowoidnich, K., & Kronfeldt, H.-D. (2010). A Prototype Hand-Held Raman Sensor for the *in situ* Characterization of Meat Quality. *Applied Spectroscopy*, *64*, 888–894.

Shi, Y., Wang, X., Borhan, M. S., Young, J., Newman, D., Berg, E., & Sun, X. (2021). A Review on Meat Quality Evaluation Methods Based on Non-Destructive Computer Vision and Artificial Intelligence Technologies. *Food Science of Animal Resources*, *41*, 563–588.

Shinzawa, H., Awa, K., Kanematsu, W., & Ozaki, Y. (2009). Multivariate data analysis for Raman spectroscopic imaging. *Journal of Raman Spectroscopy*, *40*, 1720–1725.

Sohn, W. B., Lee, S. Y., & Kim, S. (2020). Single-layer multiple-kernel-based convolutional neural network for biological Raman spectral analysis. *Journal of Raman Spectroscopy*, *51*, 414–421.

Sokolova, M., Japkowicz, N., & Szpakowicz, S. (2006). Beyond Accuracy, F-Score and ROC: A Family of Discriminant Measures for Performance Evaluation. In A. Sattar & B. Kang (Eds.), *AI 2006: Advances in Artificial Intelligence* (pp. 1015–1021). Berlin, Heidelberg: Springer.

Sowoidnich, K., Schmidt, H., Kronfeldt, H.-D., & Schwägele, F. (2012). A portable 671nm Raman sensor system for rapid meat spoilage identification. *Vibrational Spectroscopy*, *62*, 70–76.

Sowoidnich, K., Schmidt, H., Maiwald, M., Sumpf, B., & Kronfeldt, H.-D. (2010). Application of Diode-Laser Raman Spectroscopy for In situ Investigation of Meat Spoilage. *Food and Bioprocess Technology*, *3*, 878–882.

Soyer, A., Özalp, B., Dalmış, Ü., & Bilgin, V. (2010). Effects of freezing temperature and duration of frozen storage on lipid and protein oxidation in chicken meat. *Food Chemistry*, *120*, 1025–1030.

Strange, E. D., Benedict, R. C., Smith, J. L., & Swift, C. E. (1977). Evaluation of Rapid Tests for Monitoring Alterations in Meat Quality During Storage. *Journal of Food Protection*, *40*, 843–847.

Sun, X., Young, J., Liu, J.-H., & Newman, D. (2018). Prediction of pork loin quality using online computer vision system and artificial intelligence model. *Meat Science*, *140*, 72–77.

Sun, Y., Tang, H., Zou, X., Meng, G., & Wu, N. (2022). Raman spectroscopy for food quality assurance and safety monitoring: A review. *Current Opinion in Food Science*, *47*, 100910.

Taheri-Garavand, A., Fatahi, S., Omid, M., & Makino, Y. (2019). Meat quality evaluation based on computer vision technique: A review. *Meat Science*, *156*, 183–195.

Talaikis, M., Strazdaitė, S., Žiaunys, M., & Niaura, G. (2020). Far-Off Resonance: Multiwavelength Raman Spectroscopy Probing Amide Bands of Amyloid-β-(37–42) Peptide. *Molecules*, *25*, 3556.

Talari, A. C. S., Movasaghi, Z., Rehman, S., & Rehman, I. ur. (2015). Raman Spectroscopy of Biological Tissues. *Applied Spectroscopy Reviews*, *50*, 46–111.

Tan, A., Zhao, Y., Sivashanmugan, K., Squire, K., & Wang, A. X. (2019). Quantitative TLC-SERS detection of histamine in seafood with support vector machine analysis. *Food Control*, *103*, 111–118.

Tao, F., & Peng, Y. (2015). A Nondestructive Method for Prediction of Total Viable Count in Pork Meat by Hyperspectral Scattering Imaging. *Food and Bioprocess Technology*, *8*, 17–30.

Triki, M., Herrero, A. M., Jiménez-Colmenero, F., & Ruiz-Capillas, C. (2018). Quality Assessment of Fresh Meat from Several Species Based on Free Amino Acid and Biogenic Amine Contents during Chilled Storage. *Foods*, *7*, 132.

Tu, Q., & Chang, C. (2012). Diagnostic applications of Raman spectroscopy. *Nanomedicine: Nanotechnology, Biology and Medicine*, *8*, 545–558.

Uusitalo, S., Popov, A., Ryabchikov, Y. V., Bibikova, O., Alakomi, H.-L., Juvonen, R., … Laitila, A. (2017). Surface-enhanced Raman spectroscopy for identification and discrimination of beverage spoilage yeasts using patterned substrates and gold nanoparticles. *Journal of Food Engineering*, *212*, 47–54.

V, P. P., R, P., Sathe, V., & Mahalingam, U. (2019). Graphene boosted silver nanoparticles as surface enhanced Raman spectroscopic sensors and photocatalysts for removal of standard and industrial dye contaminants. *Sensors and Actuators B: Chemical*, *281*, 679–688.

Waimin, J., Gopalakrishnan, S., Heredia-Rivera, U., Kerr, N. A., Nejati, S., Gallina, N. L. F., … Rahimi, R. (2022). Low-Cost Nonreversible Electronic-Free Wireless pH Sensor for Spoilage Detection in Packaged Meat Products. *ACS Applied Materials & Interfaces*, *14*, 45752–45764.

Wand, M. P., & Jones, M. C. (1994). *Kernel Smoothing*. CRC Press.

Wang, D., Wang, X., Liu, T., & Liu, Y. (2012). Prediction of total viable counts on chilled pork using an electronic nose combined with support vector machine. *Meat Science*, *90*, 373–377.

Wang, G., Ma, F., Zeng, L., Bai, Y., Wang, H., Xu, X., & Zhou, G. (2018). Modified atmosphere packaging decreased Pseudomonas fragi cell metabolism and extracellular proteolytic activities on meat. *Food Microbiology*, *76*, 443–449.

Wang, K., Li, Z., Li, J., & Lin, H. (2021). Raman spectroscopic techniques for nondestructive analysis of agri-foods: A state-of-the-art review. *Trends in Food Science & Technology*, *118*, 490–504.

Wang, K., Yue, Z., Lin, H., Wang, Q., Wang, L., Tian, Y., & Ren, L. (2023). Rapid classification of the freshness grades of sea bass (Lateolabrax japonicus) fillets using a portable Raman spectrometer with machine learning method. *Microchemical Journal*, *192*, 108948.

Wang, P., Guo, L., Tian, Y., Chen, J., Huang, S., Wang, C., … Gao, J. (2021). Discrimination of blood species using Raman spectroscopy combined with a recurrent neural network. *OSA Continuum*, *4*, 672–687.

Wang, Q., Garrity, G. M., Tiedje, J. M., & Cole, J. R. (2007). Naïve Bayesian Classifier for Rapid Assignment of rRNA Sequences into the New Bacterial Taxonomy. *Applied and Environmental Microbiology*, *73*, 5261–5267.

Wang, W., Zhang, H., Yuan, Y., Guo, Y., & He, S. (2018). Research Progress of Raman Spectroscopy in Drug Analysis. *AAPS PharmSciTech*, *19*, 2921–2928.

Wang, X., Deng, Y., Sun, J., Ding, Y., Liu, Y., & Tian, T. (2021). Unraveling characterizations of bacterial community and spoilage profiles shift in chilled pork during refrigerated storage. *Food Science and Technology*, *42*.

Wenjiao, F., Yongkui, Z., Yunchuan, C., Junxiu, S., & Yuwen, Y. (2014). TBARS predictive models of pork sausages stored at different temperatures. *Meat Science*, *96*, 1–4.

Wiercigroch, E., Szafraniec, E., Czamara, K., Pacia, M. Z., Majzner, K., Kochan, K., … Malek, K. (2017). Raman and infrared spectroscopy of carbohydrates: A review. *Spectrochimica Acta Part A: Molecular and Biomolecular Spectroscopy*, *185*, 317–335.

Willis, A. D. (2019). Rarefaction, Alpha Diversity, and Statistics. *Frontiers in Microbiology*, 10.

Windom, B. C., & Hahn, D. W. (2013). Raman Spectroscopy. In Q. J. Wang & Y.-W. Chung (Eds.), *Encyclopedia of Tribology* (pp. 2742–2747). Boston, MA: Springer US.

Wu, Xiang, Song, X., Qiu, Z., & He, Y. (2016). Mapping of TBARS distribution in frozen–thawed pork using NIR hyperspectral imaging. *Meat Science*, *113*, 92–96.

Wu, Xiaohong, Liang, X., Wang, Y., Wu, B., & Sun, J. (2022). Non-Destructive Techniques for the Analysis and Evaluation of Meat Quality and Safety: A Review. *Foods*, *11*, 3713.

Xia, Y., & Sun, J. (2023). Alpha Diversity. *Bioinformatic and Statistical Analysis of Microbiome Data: From Raw Sequences to Advanced Modeling with QIIME 2 and R* (pp. 289–333). Cham: Springer International Publishing.

Xu, Y., Zhong, P., Jiang, A., Shen, X., Li, X., Xu, Z., … Lei, H. (2020). Raman spectroscopy coupled with chemometrics for food authentication: A review. *TrAC Trends in Analytical Chemistry*, *131*, 116017.

Yang, B., Wang, Y., & Qian, P.-Y. (2016). Sensitivity and correlation of hypervariable regions in 16S rRNA genes in phylogenetic analysis. *BMC Bioinformatics*, *17*, 135.

Yang, D., & Ying, Y. (2011). Applications of Raman Spectroscopy in Agricultural Products and Food Analysis: A Review. *Applied Spectroscopy Reviews*, *46*, 539–560.

Yang, H., Hopkins, D. L., Zhang, Y., Zhu, L., Dong, P., Wang, X., … Fowler, S. M. (2020). Preliminary investigation of the use of Raman spectroscopy to predict beef spoilage in different types of packaging. *Meat Science*, *165*, 108136.

Yang, Q., Sun, D.-W., & Cheng, W. (2017). Development of simplified models for nondestructive hyperspectral imaging monitoring of TVB-N contents in cured meat during drying process. *Journal of Food Engineering*, *192*, 53–60.

Yuan, H., Li, W., Chen, C., Yu, H., Huang, J., Lou, X., & Tian, H. (2023). The role of bacterial nanocellulose mats encapsulated with cinnamaldehyde on chilled meat preservation. *International Journal of Food Science & Technology*, *58*, 880–889.

Zając, A., Dymińska, L., Lorenc, J., & Hanuza, J. (2017). Fourier Transform Infrared and Raman Spectroscopy Studies of the Time-Dependent Changes in Chicken Meat as a Tool for Recording Spoilage Processes. *Food Analytical Methods*, *10*, 640–648.

Zapotoczny, P., Szczypiński, P. M., & Daszkiewicz, T. (2016). Evaluation of the quality of cold meats by computer-assisted image analysis. *LWT - Food Science and Technology*, *67*, 37–49.

Zhang, H., Cao, Y., Dong, X., Li, X., & Zhang, C. (2023). Effect of different postmortem ageing conditions on physicochemical properties, structure and water-holding capacity of pork. *International Journal of Food Science & Technology*, *58*, 1662–1672.

Zhang, L., & Peng, Y. (2016). Noninvasive Qualitative and Quantitative Assessment of Spoilage Attributes of Chilled Pork Using Hyperspectral Scattering Technique. *Applied Spectroscopy*, *70*, 1309–1320.

Zhang, Y., Wei, J., Yuan, Y., & Yue, T. (2019). Diversity and characterization of spoilage-associated psychrotrophs in food in cold chain. *International Journal of Food Microbiology*, *290*, 86–95.

Zhao, F., Wei, Z., Bai, Y., Li, C., Zhou, G., Kristiansen, K., & Wang, C. (2022). Proteomics and Metabolomics Profiling of Pork Exudate Reveals Meat Spoilage during Storage. *Metabolites*, *12*, 570.

Zhao, F., Wei, Z., Zhou, G., Kristiansen, K., & Wang, C. (2022). Effects of Different Storage Temperatures on Bacterial Communities and Functional Potential in Pork Meat. *Foods*, *11*, 2307.

Zheng, X., Peng, Y., & Wang, W. (2017). A Nondestructive Real-Time Detection Method of Total Viable Count in Pork by Hyperspectral Imaging Technique. *Applied Sciences*, *7*, 213.

Zhou, C., Wang, J., Li, R., & Ye, K. (2020). High-throughput sequencing analysis of the bacterial community for assessing the differences in extraction methods of bacteria separation from chilled pork. *LWT*, *134*, 110213.

Zhu, G., Zhu, X., Fan, Q., & Wan, X. (2011). Raman spectra of amino acids and their aqueous solutions. *Spectrochimica Acta Part A: Molecular and Biomolecular Spectroscopy*, *78*, 1187–1195.